

1 **How alkaline compounds control atmospheric aerosol particle acidity**

2 Vlassis A. Karydis^{1,2*}, Alexandra P. Tsimpidi^{1,2,3}, Andrea Pozzer^{1,4}, and Jos Lelieveld^{1,5}

3

4 ¹ Max Planck Institute for Chemistry, Atmospheric Chemistry Dept., Mainz, 55128, Germany.

5 ² Forschungszentrum Jülich, Inst. for Energy and Climate Research, IEK-8, Jülich, 52425, Germany.

6 ³ National Observatory of Athens, Inst. for Environmental Research and Sustainable Development, Athens, 15236, Greece.

7 ⁴ International Centre for Theoretical Physics, Trieste, 34151, Italy

8 ⁵ The Cyprus Institute, Climate and Atmosphere Research Center Nicosia, 1645, Cyprus.

9

10 *Correspondence to:* Vlassis A. Karydis (v.karydis@fz-juelich.de)

11 **Abstract.** The acidity of atmospheric particulate matter regulates its mass, composition and toxicity, and has important
12 consequences for public health, ecosystems and climate. Despite these broad impacts, the global distribution and evolution of
13 aerosol particle acidity are unknown. We used the comprehensive atmospheric multiphase chemistry – climate model EMAC
14 to investigate the main factors that control aerosol particle acidity and uncovered remarkable variability and unexpected trends
15 during the past 50 years in different parts of the world. Aerosol particle acidity decreased strongly over Europe and North
16 America during the past decades while at the same time it increased over Asia. Our simulations revealed that these particle
17 acidity trends are strongly related to changes in the phase partitioning of nitric acid, production of sulfate in aqueous aerosols,
18 and the aerosol hygroscopicity. It is remarkable that the aerosol hygroscopicity (κ) has increased in many regions
19 following the particle pH. Overall, we find that alkaline compounds, notably ammonium, and to a lesser extent crustal cations,
20 regulate the particle pH on a global scale. Given the importance of aerosol particles for the atmospheric energy budget, cloud
21 formation, pollutant deposition and public health, alkaline species hold the key to control strategies for air quality and climate
22 change.

23 **1. Introduction**

24 Aerosol particle acidity is a central property of atmospheric particulates that influence clouds, climate and air quality, including
25 impacts on human health (Raizenne et al., 1996; Lelieveld et al., 2015). It affects the partitioning of semi-volatile acids between
26 the gas and particle phases (Guo et al., 2016; Guo et al., 2017; Guo et al., 2018; Nenes et al., 2020), secondary organic aerosol
27 (SOA) formation (Xu et al., 2015; Marais et al., 2016), the solubility of trace metals in aerosol particles (Oakes et al., 2012),
28 associated with their toxicity (Fang et al., 2017) and nutrient capacity (Jickells et al., 2005), the activation of halogens that act
29 as oxidants (Saiz-Lopez and von Glasow, 2012), the conversion of sulfur dioxide (Seinfeld and Pandis, 2006; Cheng et al.,

30 2016), the particle hygroscopic growth and lifetime (Metzger et al., 2006;Abdelkader et al., 2015;Karydis et al., 2017), and
31 atmospheric corrosivity (Leygraf et al., 2016). Direct measurement of particle acidity is difficult and associated with much
32 uncertainty, being dependent on filter sampling and the H⁺ molality in the aqueous extract, which is sensitive to artifacts
33 (Pathak et al., 2004). Therefore, particle pH, a commonly used acidity metric of aqueous aerosols, is typically inferred by
34 proxy techniques (Hennigan et al., 2015;Pye et al., 2020). Two of the most common are the ion balance and the molar ratio
35 methods. These methods do not consider the effects of aerosol water and multiphase interactions with gas phase species as
36 well as the partial dissociation of acids (Hennigan et al., 2015). The simultaneous measurement of gas phase species can
37 improve particle pH estimates by accounting for the phase partitioning of semi-volatile species (e.g., NH₃, HNO₃). However,
38 the accuracy of this approach relies on the availability of information on these species in both the gas and particle phase, being
39 scant in most cases.

40 The most reliable estimates of pH are obtained with thermodynamic equilibrium models, although the accuracy can be limited
41 by not accounting for all ionic species. For example, most atmospheric chemistry models do not consider crustal elements
42 (e.g., Ca²⁺, Mg²⁺, K⁺) and Na⁺ in sea salt. These species affect the ion balance by influencing the phase partitioning of nitrate
43 and ammonium, especially in areas where aeolian dust is abundant (Karydis et al., 2016). Here we present 50-year global
44 acidity trends of fine particulate matter (i.e. with a diameter < 2.5 μm) by employing the EMAC chemistry – climate model
45 (Jöckel et al., 2010). The pH calculations are performed online with the ISORROPIA II thermodynamic equilibrium model
46 (Fountoukis and Nenes, 2007).

47 **2. Results and Discussion**

48 **2.1 Global variability of aerosol particle acidity**

49 Figure 1 shows the modeled near-surface distribution of fine aerosol particle acidity for the 2010-2015 period. We find
50 predominantly acidic particles over the anthropogenically influenced regions in the northern hemisphere and the tropical
51 biomass burning zones, and mostly alkaline particles over deserts and oceans, especially over the southern oceans. The pH
52 typically ranges from 4.0 to 6.7 (5.3 on average) over the western USA since it is affected by crustal cations from the
53 surrounding deserts. Polluted areas located downwind of crustal sources are of special interest since the pH calculations can
54 be sensitive to the aerosol state assumption (see section 4.3). Over Pasadena, the base case model using the stable state mode
55 estimates a mean pH of 5.9 units, while the sensitivity simulation with only liquid particles results in 2.7 pH units (equal to
56 Guo et al. (2017) estimations by using the metastable assumption; Table A1). Our sensitivity analysis revealed that the aerosol
57 state itself is not affected by the state assumption since both stable and metastable predict the same amount of water in the
58 aerosol. Differences in the calculated pH can be due to the high concentrations of calcium from the Great Basin Desert which
59 results in the precipitation of high amounts of CaSO₄, lowering the particle acidity (but without affecting the water activity
60 since CaSO₄ is insoluble and does not contribute to the MDRH depression). It is worth mentioning that calcium was not

61 included in the Guo et al. (2017) study which helps explain the differences in the observed and simulated particle acidity. The
62 simulated particle-phase fraction of nitrate over Pasadena is 40% using the stable state assumption and 32% using the
63 metastable assumption, compared to the observationally derived 51%. Over Europe, the pH ranges from 2.6 to 6.7 (3.9 on
64 average). Observational estimates of particle pH from the Po Valley (Squizzato et al., 2013; Masiol et al., 2020) and Cabauw
65 (Guo et al., 2018) support the relatively low acidity of fine particles over Europe (Table A1). Model calculations compare well
66 with observational estimates from Cabauw, however, result in higher pH (~1 unit) compared to values from Po Valley
67 (estimated by using the E-AIM model). Over East Asia the average pH is 4.7, ranging from 2.6 to 7.4. Relatively high pH are
68 found over regions where anthropogenic aerosols are mixed with aeolian dust, e.g., from the Gobi Desert, which decrease the
69 acidity (e.g., ~6 pH units over Hohhot, which agrees well with the estimations of Wang et al. (2019a)). The relatively low pH
70 in large parts of Asia is explained by strong SO₂ emissions and associated sulfate, which have increased strongly in the past
71 decades (e.g., over Guangzhou, supported by estimations of Jia et al. (2018)). Estimates of unrealistically high particle acidity
72 can result from omitting the gas phase concentrations of semi-volatile ions from the pH calculations (e.g., estimates over Hong
73 Kong (Yao et al., 2007; Xue et al., 2011), Singapore (Behera et al., 2013) and Shanghai (Pathak et al., 2009); Table A1). At
74 the same time, SO₂ emissions have decreased over Europe and USA, and recently in China. However, aerosol particles over
75 the eastern USA have remained acidic, with an average pH of 3.0 until recently, corroborating the findings of Weber et al.
76 (2016) and Lawal et al. (2018) that aerosol particle acidity over this region is less sensitive to SO₂ than to NH₃ emissions.
77 The particle pH over polluted northern hemispheric mid-latitudes (e.g., over East Asia) and the northern extratropical oceans
78 exhibits a clear seasonal pattern with lower values during boreal summer and higher ones during winter, driven by the
79 availability of ammonium and by the aerosol water content (Fig. 2). This is evident from both our model calculations and from
80 observational estimates mostly in heavily populated areas such as the Po Valley (Squizzato et al., 2013), Beijing (Tan et al.,
81 2018), and Tianjin (Shi et al., 2017), and to a lesser extent over areas strongly affected by aeolian dust (e.g., Hohhot; Wang et
82 al., 2019b) (Table A1). Over tropical regions, fine particulates have a pH between 3.2 and 7.4, being strongly influenced by
83 pyrogenic potassium, i.e., from widespread biomass burning (Metzger et al., 2006), and a high aerosol water content.
84 Observational estimates from Sao Paulo support these high pH values (Vieira-Filho et al., 2016), albeit with 1 unit bias mainly
85 related to the use of the E-AIM model. Over deserts, particles are relatively alkaline, with a pH up to 7.4. Particles in the
86 marine environment tend to be alkaline also, with a pH up to 7.4 over the southern oceans. Observational estimates report
87 highly acidic particles over the southern oceans due to the lack of gas phase input for the pH calculations (Dall'Osto et al.,
88 2019). Over the Arctic and the northern Atlantic and Pacific Oceans, particle acidity is significantly enhanced by strong sulfur
89 emissions from international shipping and pollution transport from industrialized areas (Fig. 1). The pH over the northern
90 extratropical oceans and the Arctic ranges from 2.0 to 7.0 with an average of about 5.2. The annual cycle of particle acidity
91 over these regions is strongly influenced by anthropogenic pollution, being relatively high during boreal summer. Over the
92 Antarctic, particle pH ranges from 4.5 to 7.0 and follows a clear seasonal pattern (Fig. 2).

93 **2.2 Temporal evolution of aerosol particle acidity**

94 Figure 1 and Table 1 present the aerosol particle pH over the period 1970-2020. We investigated the impacts of alkaline species
95 by omitting the emissions of ammonia and mineral cations in two sensitivity simulations.

96 **2.2.1 Europe**

97 Over Europe, the pH has increased strongly from about 2.8 during the 1970s to 3.9 recently. Especially during the 1990s NH₃
98 emissions over Europe increased significantly by 14%, while at the same time NO_x and SO₂ emissions decreased by 13% and
99 49%, respectively. While this trend has continued in the past decade, pH changes slowed because the sulfate and nitrate
100 decreases have been compensated through volatilization of ammonia from the particles. In addition, the recently increasing
101 cation/anion ratio is accompanied by a reduction of aerosol water, preventing a significant decrease of the particle acidity (Fig.
102 S1). Overall, the increase of aerosol particle pH by more than 1 unit during the last 50 years had a significant impact on the
103 gas-particle partitioning of semi-volatile acids, e.g., nitric acid, since their dissociation into ions enhances their solubility (Nah
104 et al., 2018). Here, the fraction of nitrate in the particle phase relative to total nitrate (gas plus particle) has increased from
105 ~70% to 85% (Fig. 3). The increase in particle pH has been accompanied by an increase in aerosol kappa hygroscopicity (Fig.
106 4). After the substantial reduction of SO₂ emissions, sulfate salts (e.g., ammonium sulfate with kappa=0.53) are replaced by
107 more hygroscopic nitrate salts (e.g., ammonium nitrate with kappa=0.67) in the aerosol composition. In addition, the decrease
108 of organic compound emissions during the last 50 years contributed to the increase of the aerosol hygroscopicity. Our
109 sensitivity simulations reveal that particle acidity over Europe is highly sensitive to NH₃ emissions. Despite the decline of both
110 SO₂ and NO_x during the past decades, the particle would have remained highly acidic (pH ~1) in the absence of NH₃.

111 **2.2.2 North America**

112 Over North America, particle acidity also decreased with SO₂ and NO_x emissions. Nevertheless, these emissions are still
113 relatively strong in the eastern USA (5 times higher than in the western USA) resulting in very acidic particles, with a pH
114 ranging from 2.2 in 1971 to 3.3 recently (Figs. 1 and S1). Such acidic conditions promote the dissolution of metals (e.g., Fe,
115 Mn, Cu) in ambient particles (Fang et al., 2017). Soluble transition metals in atmospheric aerosols have been linked to adverse
116 health impacts since they generate reactive oxygen species, leading to oxidative stress and increased toxicity of fine particulate
117 matter (Fang et al., 2017; Park et al., 2018). Since the solubility of transition metals increases exponentially below a pH of 3,
118 the decrease of particle acidity over the eastern USA reported here suggests that the particles have become substantially less
119 toxic in the past few decades. Similar to Europe, the increasing pH has resulted in a growing aerosol nitrate fraction from
120 ~50% during the 1970s to 65% recently (Fig. 3), and to a strong increase of aerosol hygroscopicity by ~0.15 units at the cloud
121 base (Fig. 4). The role of NH₃ is critically important; without it the particle pH over the eastern USA would be close to zero.
122 Over the western USA, the particle pH is higher (~5), being affected by aeolian dust from the Great Basin Desert, although
123 NH₃ is still the most important alkaline buffer.

124 **2.2.3 East and South Asia**

125 In Asia, SO₂ and NO_x emissions have increased drastically since 1970. However, the simultaneous increase of NH₃ emissions
126 along with the presence of mineral dust from the surrounding deserts (i.e., Gobi, Taklimakan, Thar) decelerated the increase
127 of particle acidity. Over East Asia, the particle pH decreased from about 5.3 during the 1970s to 4.5 in 2010. This change in
128 particle acidity has affected the predominant pathway of sulfate formation through aerosol aqueous phase chemistry. Under
129 acidic conditions, SO₂ is mainly oxidized by transition metal ions, while at pH > 5 the oxidation by O₃ and NO₂ predominates
130 (Cheng et al., 2016). Therefore, the decrease of pH during the last 50 years, even though being relatively modest, was sufficient
131 to turn-off sulfate production from O₃ oxidation (Fig. 5). At the same time, the increased particle acidity hinders the partitioning
132 of nitric acid to the particle phase, reducing the aerosol nitrate fraction from 90% to 80% (Fig. 3). Remarkably, the aerosol
133 hygroscopicity has increased from ~0.3 in the 1970s to 0.45 recently (Fig. 4), revealing a reverse development compared to
134 Europe and the USA. Here, the fraction of mineral dust in the aerosol is higher; therefore, the particles gained hygroscopicity
135 by the acquired pollution solutes. Recently, the SO₂ emissions have dropped and the NO_x emission increase has slowed in
136 East Asia, while SO₂ emissions are soaring in South Asia. SO₂ emission trends since 2007 have been so drastic that inventories
137 and scenarios tend to overestimate the emitted SO₂. Satellite observations indicate that India has recently overtaken China as
138 the world largest emitter of SO₂ (Li et al., 2017). Following the satellite observations, we implemented the significant SO₂
139 reduction trends into our model (Fig. S2). Surprisingly, the effect only becomes noticeable over East Asia after 2016, when the
140 particle pH started increasing by about 0.3 units, while we do not find any change over South Asia. This corroborates the
141 strong buffering that we found over other regions such as Europe. Fig. 1 shows that NH₃ has been the major buffer, supporting
142 the recent findings of Zheng et al. (2020) that the acid-base pair of NH₄⁺/NH₃ provides the largest buffering capacity over East
143 and South Asia. However, we also found that in East Asia and to a lesser extent in South Asia crustal elements, not considered
144 in the study of Zheng et al. (2020), have contributed significantly on maintaining a mean pH of 4.5 – 5 in the past decade (Fig.
145 1). Calcium is the major crustal component of dust from the Gobi and Taklimakan deserts (Karydis et al., 2016) and unlike
146 other crustal compounds it can react with sulfate ions and form insoluble CaSO₄, which precipitates out of the aerosol aqueous
147 phase. This interaction reduces the aqueous sulfate and thus the particle acidity.

148 **2.2.4 Tropical forests, Middle East**

149 Over tropical forests, aerosol particles are typically not very acidic with pH values >4. Note that organic acids were not
150 included in the particle pH calculations, however, their contribution to the total ionic load is small (Andreae et al.,
151 1988;Falkovich et al., 2005), and particle acidity can be attributed to inorganic acids. Over the Amazon and Congo basins, the
152 particle pH remained around 5 since 1970. The Southeast Asian forest atmosphere is affected by pollution from mainland Asia,
153 and the particle pH decreased to around 4 recently. This pH drop has enhanced SOA formation from isoprene, since under
154 low-NO_x conditions (typical over rainforests) the presence of acidifying sulfate increases the reactive uptake of epoxydiols
155 (Xu et al., 2015;Surratt et al., 2010). Nevertheless, NH₃ emissions provide a remarkably strong buffer over all three tropical

156 regions while mineral dust cations are also important over the Amazon and Congo forests. Further, the Middle East is affected
157 by strong anthropogenic (fossil fuel related) and natural (aeolian dust) aerosol sources. Due to the high abundance of mineral
158 dust, the pH has remained close to 7. Without crustal cations, the pH would drop to about 4. Despite the omnipresence of
159 alkaline species from the surrounding deserts, NH_3 still plays a central role in controlling the acidification of mineral dust
160 aerosols, which can affect their hygroscopic growth and hence their climate forcing (Klingmuller et al., 2019;Klingmüller et
161 al., 2020).

162 **2.2.5 Oceans**

163 Over the Arctic and northern extra-tropical oceans, particle acidity is strongly affected by pollution transport from the urban-
164 industrial mid-latitudes. The Arctic particle pH is highly variable, remaining relatively low up to 1990 (~4.2), after which it
165 increased to about 5.2. Crustal cations are found to play a significant role lowering the particle acidity. Over the northern extra-
166 tropical oceans, particle pH has remained relatively constant (~4.8). NH_3 provides an important alkaline buffer, and without it
167 the particle pH would have been below 3. NH_3 is also proved to be important over the tropical and southern extra-tropical
168 oceans, where a noticeable increase in aerosol particle acidity occurred after June 1991, when the eruption of Mount Pinatubo
169 in the Philippines released ~20 million tons of SO_2 into the stratosphere (McCormick et al., 1995). The impact of Pinatubo
170 sulfate, after returning to the troposphere, on particle acidity is mostly evident over Antarctica, where the pH dropped by 2
171 units, as the stratospheric circulation is strongest in the winter hemisphere. Over Antarctica concentrations of dust and
172 especially of NH_3 are very low, and Fig. 1 illustrates that only in this pristine environment the large Pinatubo anomaly could
173 overwhelm the buffering by alkaline species. Except after Pinatubo, the pH has remained nearly constant at 5.8 over Antarctica
174 and about 5.5 in the tropics and 6.8 in the southern extra-tropics.

175 **3. Conclusions**

176 We find that over Europe and North America the aerosol particle acidity decreased strongly in the past few decades resulting
177 in substantially less toxic and more hygroscopic aerosols. At the same time, the particle acidity over Asia has increased, even
178 though the increase of NH_3 emissions and the presence of mineral dust decelerated the change in the particle pH. The inevitable
179 decrease of the particle pH hindered the partitioning of nitric acid into the particulate phase and the sulfate production in the
180 aerosol aqueous phase; however, the aerosol hygroscopicity increased over Asia following a reverse correlation with the
181 particle pH. Overall, the aerosol particle pH is generally well-buffered by alkaline compounds, notably NH_3 and in some areas
182 crustal elements. NH_3 is found to supply remarkable buffering capacity on a global scale, from the polluted continents to the
183 remote oceans. In the absence of NH_3 , aerosol particles would be highly (to extremely) acidic in most of the world. Therefore,
184 potential future changes in NH_3 are critically important in this respect. Agriculture is the main NH_3 source and a controlling
185 factor in fine particle concentrations and health impacts in some areas (e.g., Europe) (Pozzer et al., 2017). The control of
186 agricultural ammonia emissions must therefore be accompanied by very strong reductions of SO_2 and NO_x to avoid that aerosol

187 particles become highly acidic with implications for human health (aerosol toxicity), ecosystems (acid deposition and nutrient
188 availability), clouds and climate (aerosol hygroscopicity).

189 **4. Appendix A: Materials and Methods**

190 **4.1 Aerosol-chemistry-climate model**

191 We used the ECHAM5/MESSy Atmospheric Chemistry (EMAC) model, which is a numerical chemistry and climate
192 simulation system that describes lower and middle atmosphere processes (Jöckel et al., 2006). EMAC uses the Modular Earth
193 Submodel System (MESSy2) (Jöckel et al., 2010) to link the different sub-models with an atmospheric dynamical core, being
194 an updated version of the 5th generation European Centre - Hamburg general circulation model (ECHAM5) (Roeckner et al.,
195 2006). EMAC has been extensively described and evaluated against in situ observations and satellite retrievals to compute
196 particulate matter concentrations and composition, aerosol optical depth, acid deposition, gas phase mixing ratios, cloud
197 properties, and meteorological parameters (Karydis et al., 2016; Pozzer et al., 2012; Tsimpidi et al., 2016; Karydis et al.,
198 2017; Bacer et al., 2018). The spectral resolution of EMAC used in this study is T63L31, corresponding to a horizontal grid
199 resolution of approximately $1.9^\circ \times 1.9^\circ$ and 31 vertical layers extending up to 10 hPa (i.e., 25 km) from the surface. The presented
200 model simulations encompass the 50-year period 1970-2020.

201 EMAC calculates fields of gas phase species online through the Module Efficiently Calculating the Chemistry of the
202 Atmosphere (MECCA) Submodel (Sander et al., 2019). MECCA calculates the concentration of a range of gases, including
203 aerosol precursor species (e.g. SO_2 , NH_3 , NO_x , DMS, H_2SO_4 and DMSO) and the major oxidant species (e.g. OH, H_2O_2 , NO_3 ,
204 and O_3). Aerosol microphysics are calculated by the Global Modal-aerosol eXtension (GMXe) module (Pringle et al., 2010).
205 The organic aerosol formation and atmospheric evolution are calculated by the ORACLE Submodel (Tsimpidi et al., 2014,
206 2018). The aerosol size distribution is described by seven lognormal modes: four hydrophilic modes that cover the aerosol size
207 spectrum of nucleation, Aitken, accumulation and coarse modes, and three hydrophobic modes that cover the same size range
208 except nucleation. The aerosol composition within each size mode is uniform (internally mixed), however, it varies between
209 modes (externally mixed). Each mode is defined in terms of total number concentration, number mean radius, and geometric
210 standard deviation (Pringle et al., 2010). The removal of gas and aerosol species through wet and dry deposition is calculated
211 within the SCAV (Tost et al., 2006) and DRYDEP (Kerkweg et al., 2006) submodels, respectively. The sedimentation of
212 aerosols is calculated within the SEDI submodel (Kerkweg et al., 2006). The cloud cover, microphysics and precipitation of
213 large scale clouds is calculated by the CLOUD Submodel (Roeckner et al., 2006) which uses a two-moment stratiform
214 microphysical scheme (Lohmann and Ferrachat, 2010), and describes liquid droplet (Karydis et al., 2017) and ice crystal (Bacer
215 et al., 2018) formation by accounting for the aerosol physicochemical properties. The effective hygroscopicity parameter κ is
216 used to describe the influence of chemical composition on the cloud condensation nuclei (CCN) activity of atmospheric
217 aerosols. κ is calculated using the mixing rule of Petters and Kreidenweis (Petters and Kreidenweis, 2007) and the individual

218 κ parameter values for each inorganic salt (Petters and Kreidenweis, 2007; Sullivan et al., 2009). Organic aerosol species are
219 assumed to have a constant hygroscopicity kappa parameter of 0.14 while bulk mineral dust and black carbon are assumed to
220 have zero hygroscopicity.

221 **4.2 Emissions**

222 The vertically distributed (Pozzer et al., 2009) CMIP5 RCP8.5 emission inventory (van Vuuren et al., 2011) is used for the
223 anthropogenic and biomass burning emissions during the years 1970-2020. Direct emissions of aerosol components from
224 biofuel and open biomass burning are considered by using scaling factors applied on the emitted black carbon based on the
225 findings of Akagi et al. (Akagi et al., 2011) (Table S1). Dust emission fluxes and emissions of crustal species (Ca^{2+} , Mg^{2+} , K^+ ,
226 Na^+) are calculated online as described by Klingmuller, et al. (Klingmuller et al., 2018) and based on the chemical composition
227 of the emitted soil particles in every grid cell (Karydis et al., 2016); Table S2. NO_x produced by lightning is calculated online
228 and distributed vertically based on the parameterization of Grewe, et al. (Grewe et al., 2001). The emissions of NO from soils
229 are calculated online based on the algorithm of Yienger and Levy (Yienger and Levy, 1995). The oceanic DMS emissions are
230 calculated online by the AIRSEA Submodel (Pozzer et al., 2006). The natural emissions of NH_3 are based on the GEIA
231 database (Bouwman et al., 1997). Emissions of sea spray aerosols (assuming a composition suggested by Seinfeld and Pandis
232 (Seinfeld and Pandis, 2006); Table S1) and volcanic degassing emissions of SO_2 are based on the offline emission data set of
233 AEROCOM (Dentener et al., 2006).

234

235 **4.3 Thermodynamic model**

236 The inorganic aerosol composition, which is of prime importance for the accurate pH calculation, is computed with the
237 ISORROPIA-II thermodynamic equilibrium model (Fountoukis and Nenes, 2007). ISORROPIA-II calculates the
238 gas/liquid/solid equilibrium partitioning of the K^+ - Ca^{2+} - Mg^{2+} - NH_4^+ - Na^+ - SO_4^{2-} - NO_3^- - Cl^- - H_2O aerosol system and considers the
239 presence of 15 aqueous phase components and 19 salts in the solid phase. ISORROPIA-II solves for the equilibrium state by
240 considering the chemical potential of the species and minimizes the number of equations and iterations required by considering
241 specific compositional “regimes”. The assumption of thermodynamic equilibrium is a good approximation for fine-mode
242 aerosols that rapidly reach equilibrium. However, the equilibrium timescale for large particles is typically larger than the time
243 step of the model (Meng and Seinfeld, 1996) leading to errors in the size distribution of semi-volatile ions like nitrate. Since
244 the current study include reactions of nitric acid with coarse sea-salt and dust aerosol cations, the competition of fine and
245 coarse particles for the available nitric acid can only be accurately represented by taking into account the kinetic limitations
246 during condensation of HNO_3 in the coarse mode aerosols. To account for kinetic limitations by mass transfer and transport
247 between the gas and particle phases, the process of gas/aerosol partitioning is calculated in two stages (Pringle et al., 2010).
248 First, the gaseous species that kinetically condense onto the aerosol phase within the model timestep are calculated assuming

249 diffusion limited condensation (Vignati et al., 2004). Then, ISORROPIA-II re-distributes the mass between the gas and the
250 aerosol phase assuming instant equilibrium between the two phases.

251 ISORROPIA-II is used in the forward mode, in which the total (i.e., gas and aerosol) concentrations are given as input.
252 Reverse mode calculations (i.e. when only the aerosol phase composition is known) should be avoided since they are sensitive
253 to errors and infer bimodal behaviour with highly acidic or highly alkaline particles, depending on whether anions or cations
254 are in excess (Song et al., 2018). While it is often assumed that aerosols are in a metastable state (i.e., composed only of a
255 supersaturated aqueous phase), here we use ISORROPIA-II in the thermodynamically stable state mode where salts are
256 allowed to precipitate once the aqueous phase becomes saturated. For this purpose, we have used the revised ISORROPIA-II
257 model which includes modifications proposed by Song et al. (2018), who resolved coding errors related to pH calculations
258 when the stable state assumption is used. By comparing with the benchmark thermodynamic model E-AIM, Song et al. (2018)
259 found that ISORROPIA-II produces somewhat higher pH (by 0.1-0.7 units, negatively correlated with RH). However, E-AIM
260 model versions either lack crustal cations from the ambient mixture of components (e.g. version II) (Clegg et al., 1998), or
261 only include Na^+ with the restriction that it should be used when $\text{RH} > 60\%$ (e.g. version IV) (Friese and Ebel, 2010). Song et
262 al. (2018) applied the revised ISORROPIA-II during winter haze events in eastern China and found that the assumed particle
263 phase state, either stable or metastable, does not significantly impact the pH predictions.

264 We performed a sensitivity simulation with only liquid particles (i.e., metastable), which revealed that the assumed particle
265 phase state does not significantly impact the pH calculations over oceans and polluted regions (e.g., Europe), however, the
266 metastable assumption produces more acidic particles (up to 2 units of pH) in regions affected by high concentrations of crustal
267 cations and consistently low RH values (Fig. S3). Fountoukis et al. (2007) have shown that the metastable solution predicts
268 significant amounts of water below the mutual deliquescence relative humidity (MDRH, where all salts are simultaneously
269 saturated with respect to all components). Further, the generally high calcium concentrations downwind of deserts results in
270 increasing pH values due to the precipitation of insoluble salts such as the CaSO_4 . The metastable state assumption fails to
271 reproduce this since it treats only the ions in the aqueous phase. In general, high amounts of crustal species can significantly
272 increase the particle pH which is consistent with the presence of excess carbonate in the particle phase (Meng et al., 1995). It
273 is worth mentioning that the stable state solution algorithm of ISORROPIA II starts with assuming a dry aerosol, and based
274 on the ambient RH dissolves each of the salts depending on their DRH. However, in the ambient atmosphere, when the RH
275 over a wet particle is decreasing, it may not crystallize below the MDRH but instead remain in a metastable state affecting the
276 uptake of water by the particle and thus the pH. This could be the case in some locations with high diurnal variations of RH.
277 Our sensitivity calculations show that, overall, the stable state assumption produces an about 0.5 units higher global average
278 pH than the metastable assumption. Karydis et al. (2016) have shown that while the aerosol state assumption has a marginal
279 effect on the calculated nitrate aerosol tropospheric burden (2% change), it can be important over and downwind of deserts at
280 very low RHs where nitrate is reduced by up to 60% by using the metastable assumption. This is in accord with the findings
281 of Ansari and Pandis (2000) who suggested that the stable state results in higher concentrations of aerosol nitrate when the RH
282 is low (<35 %) and/or sulfate to nitrate molar ratios are low (<0.25).

283 4.4 pH calculations

284 The pH is defined as the negative decimal logarithm of the hydrogen ion activity ($a_{H^+} = \gamma x_{H^+}$) in a solution:

$$285 \quad pH = -\log_{10}(\gamma x_{H^+}) \quad (A1)$$

286 where x_{H^+} is the molality of hydrogen ions in the solution and γ is the ion activity coefficient of hydrogen. Assuming that γ
287 is unity, the aerosol particle pH can be calculated by using the hydrogen ion concentration in the aqueous particle phase
288 calculated by ISORROPIA-II (in mole m⁻³) and the aerosol water content calculated by GMXe (in mole Kg⁻¹). GMXe assumes
289 that particle modes are internally mixed and takes into account the contribution of both inorganic and organic (based on the
290 organic hygroscopicity parameter, kappa=0.14 (Tsimpidi et al., 2014)) species to aerosol water.

291 The aerosol particle pH is calculated online at each timestep, and output stored every five hours based on instantaneous
292 concentrations of fine aerosol water and hydrogen ions. The average pH values shown in the manuscript are based on the
293 calculated instantaneous mean pH values. According to the Jensen's inequality (Jensen, 1906), the average of the instantaneous
294 pH values is less than or equal to the pH calculated based on the average of the water and hydrogen ion instantaneous values.
295 We estimate that the average pH calculated based on 5-hourly instantaneous values is approximately 1-3 (~2 globally averaged)
296 units higher than the pH calculated based on the average water and hydrogen ion concentrations. By including online gas-
297 particle partitioning calculations of the NH₃/HNO₃ system in polluted air, as applied here, we find that the particle pH is higher
298 by approximately one unit (Guo et al., 2015). Hence by neglecting these aspects the particle pH would be low-biased by about
299 3 units.

300

301 4.5 Comparison against pH estimations from field derived PM_{2.5} compositional data

302 The pH calculated here is compared against pH estimations from field derived PM_{2.5} compositional data around the world
303 compiled by Pye et al. (2020) (Table A1). pH data derived from other particle sizes (e.g., PM₁) has been omitted since particle
304 acidity can vary significantly with size (Zakoura et al., 2020). It should be emphasized that the comparison presented in Table
305 A1 aims to corroborate the spatial variability of pH found in this study and not to evaluate the model calculations. Since direct
306 measurements of particle acidity are not available, the observation-based particle pH is estimated by employing
307 thermodynamic equilibrium models (e.g., ISORROPIA) and making assumptions that can significantly affect the results,
308 especially when the data are averaged over extended periods, while RH conditions during data collection are not always
309 accounted for, e.g. in studies based on filter sampling. The calculation of aerosol particle acidity on a global scale requires the
310 advanced treatment of atmospheric aerosol chemical complexity, representing the real atmosphere, and beyond the
311 conventional methods used by chemistry-climate models (CCM). The atmospheric chemistry model system EMAC is an ideal
312 tool for this purpose since it is one of the most comprehensive CCM containing advanced descriptions of the aerosol

313 thermodynamics (including e.g. dust-pollution interactions) and organic aerosol formation and atmospheric aging (affecting
314 the aerosol water). Our model calculations for aerosol particle acidity are based on some processes/factors that are not included
315 explicitly, usually neglected by model calculations used to constrain the particle acidity from observations. Sources of
316 discrepancy between the pH calculations can be the following:

- 317 • The stable/metastable assumption does not affect the pH most of the time, however, in some cases with low RHs and the
318 presence of crustal cations, the metastable assumption results in lower pHs (see section 4.3).
- 319 • Crustal species from deserts and Na^+ from sea salt can elevate the pH significantly in some locations, however, these are
320 often neglected in observations.
- 321 • The organic aerosols (which are treated comprehensively by our model using the module ORACLE and the volatility
322 basis set framework (Tsimpidi et al., 2014)) can contribute significantly to the aerosol water, and thus increase the particle
323 pH. This contribution is not considered by many observational studies.
- 324 • Including gas phase species (e.g., NH_3 , HNO_3) in the pH calculations is important. Using only the aerosol-phase as input
325 (i.e., reverse mode) the inferred pH exhibits bimodal behaviour with very acidic or alkaline values depending on whether
326 anions or cations are in excess (Hennigan et al., 2015). Even if the forward mode is used (without gas phase input), the
327 calculated particle pH is biased low (approximately 1 pH unit) due to the repartition of semi-volatile anions (i.e., NH_3)
328 to the gas phase to establish equilibrium (Guo et al., 2015).
- 329 • Another important aspect, not explicitly mentioned in many studies, relates to the methods used to derive the campaign-
330 average (or for 3D models the simulated average) pH. In our model the particle pH is calculated online (2-minute time
331 resolution), while output is stored every five hours based on instantaneous concentrations of fine particle H_2O and H^+ .
332 This mimics 5-hourly aerosol sampling. Then, the average pH values are calculated from the instantaneous mean pH
333 values (see section 4.4). Often models use average values (and not instantaneous) as output, or field-derived pH
334 calculations use average observed H_2O and H^+ values, which can result in important underestimation (by ~ 1 -3 units) of
335 the particle pH (Jensen, 1906).
- 336 • Some unrealistically high pH values in a few past studies resulted from coding errors in the stable state assumption of the
337 ISORROPIA II model, which have been corrected in our study following the recommendation of Song et al. (2018).
- 338 • The type of thermodynamic model used is also important. Song et al. (2018) found that ISORROPIA-II produces
339 somewhat higher pH (by 0.1-0.7 units, negatively correlated with RH) compared to the thermodynamic model E-AIM,
340 which is used to observationally-constrain pH in some studies.
- 341 • Measurements of $\text{PM}_{2.5}$ nitrate are not always reliable because of artifacts associated with the volatility of ammonium
342 nitrate (Schaap et al., 2004). Ammonium and nitrate can partially evaporate from Teflon filters at temperatures between
343 15 to 20 °C and can evaporate completely at temperatures above. The evaporation from quartz filters is also significant
344 at temperatures higher than 20 °C. This systematic underestimation of ammonium nitrate can affect the observed chemical
345 composition of the aerosol and thus the pH calculations.

346 • The comparison between global model output and observations at specific locations. This also concerns the aerosol
 347 concentrations but is especially important for the aerosol particle acidity. Apart from the size of the model grid cells (i.e.,
 348 $\sim 1.9^\circ \times 1.9^\circ$), the altitude is also important. The first vertical layer of EMAC is approximately 67m in height. On the other
 349 hand, ground observations are typically collected in a height up to 3 m. While the aerosol particles within size modes
 350 simulated in our model are well-mixed, perhaps this is not the case for the aerosol particles observed at the surface and
 351 potentially close to sources, and thus the particle acidity may be higher (e.g., due to the higher contribution from local
 352 primary sources like SO_4^{2-} , lower water amounts in the aerosol, or lower concentrations of semi-volatile cations like
 353 NH_4^+)
 354

355 4.6 Partitioning of nitric acid between the gas and aerosol phases

356 The impact of pH on the fraction of nitrate in the particle phase relative to total nitrate (gas plus particle), i.e., $\varepsilon(\text{NO}_3^-)$, during
 357 the 50 years of simulation in specific regions is calculated as follows (Nah et al., 2018):

$$358 \quad \varepsilon(\text{NO}_3^-) = \frac{H_{\text{HNO}_3}^* WRT(0.987 \times 10^{-14})}{\gamma_{\text{NO}_3^-} \gamma_{\text{H}^+} 10^{-\text{pH}} + H_{\text{HNO}_3}^* WRT(0.987 \times 10^{-14})} \quad (\text{A2})$$

359 Where $H_{\text{HNO}_3}^*$ is the combined molality-based equilibrium constant of HNO_3 dissolution and deprotonation, γ 's represent the
 360 activity coefficients, W is the aerosol water, R is the gas constant, and T is the ambient temperature. Eq. A2 is equivalent with
 361 the instantaneous calculations of ISOROPIA II within EMAC. However, the model output is produced after considering all
 362 processes in the model and is not calculated at every timestep. Therefore, the use of Eq. 2 can provide a clearer picture of the
 363 impact of pH on HNO_3 gas/particle partitioning since the model output (e.g., gas-phase HNO_3 and nitrate in 4 size modes) is
 364 subject to uncertainties related to other processes (e.g., deposition, coagulation, transport, etc.).

365 4.7 Sulfate formation in aqueous aerosols

366 The sulfate production rate on aqueous particles from the heterogeneous oxidation of S(IV) with the dissolved O_3 is given by

$$367 \quad R_0 = k [\text{O}_3] \quad (\text{A3})$$

368 . The first-order uptake rate, k , from monodisperse aerosols with radius r_a and total aerosol surface A , is calculated following
 369 Jacob (Jacob, 2000):

$$370 \quad k = \left(\frac{r_a}{D_g} + \frac{4}{v\gamma} \right)^{-1} A \quad (\text{A4})$$

372 where v is the mean molecular speed of O_3 and D_g is its gas-phase molecular diffusion coefficient calculated as follows:

373
$$D_g = \frac{9.45 \times 10^{17} \times \sqrt{T \left(3.47 \times 10^{-2} + \frac{1}{M} \right)}}{\rho_{air}} \quad (A5)$$

374 where T is the ambient air temperature, ρ_{air} is the air density, and M the molar mass of O_3 . γ is the reaction probability calculated
 375 following Jacob (Jacob, 2000) and Shao et al. (Shao et al., 2019).

376
$$\gamma = \left(\frac{1}{\alpha} + \frac{v}{4HRT\sqrt{D_a K} f_r} \right) \quad (A6)$$

377 where α is the mass accommodation coefficient, D_a is the aqueous-phase molecular diffusion coefficient of O_3 , H is the
 378 effective Henry's law constant of O_3 (Sander, 2015), R is the ideal gas constant, f_r is the reacto-diffusive correction term (Shao
 379 et al., 2019), and K is the pseudo-first order reaction rate constant between $S(IV)$ and O_3 in the aqueous phase (Seinfeld and
 380 Pandis, 2006).

381

382 5. References

- 383 Abdelkader, M., Metzger, S., Mamouri, R. E., Astitha, M., Barrie, L., Levin, Z., and Lelieveld, J.: Dust-air pollution dynamics
 384 over the eastern Mediterranean, *Atmospheric Chemistry and Physics*, 15, 9173-9189, 10.5194/acp-15-9173-2015, 2015.
- 385 Akagi, S. K., Yokelson, R. J., Wiedinmyer, C., Alvarado, M. J., Reid, J. S., Karl, T., Crouse, J. D., and Wennberg, P. O.:
 386 Emission factors for open and domestic biomass burning for use in atmospheric models, *Atmospheric Chemistry and*
 387 *Physics*, 11, 4039-4072, 10.5194/acp-11-4039-2011, 2011.
- 388 Andreae, M. O., Talbot, R. W., Andreae, T. W., and Harriss, R. C.: Formic and acetic acid over the central Amazon region,
 389 Brazil. 1. dry season, *Journal of Geophysical Research-Atmospheres*, 93, 1616-1624, 10.1029/JD093iD02p01616, 1988.
- 390 Ansari, A. S., and Pandis, S. N.: The effect of metastable equilibrium states on the partitioning of nitrate between the gas and
 391 aerosol phases, *Atmospheric Environment*, 34, 157-168, 10.1016/s1352-2310(99)00242-3, 2000.
- 392 Bacer, S., Sullivan, S. C., Karydis, V. A., Barahona, D., Kramer, M., Nenes, A., Tost, H., Tsimpidi, A. P., Lelieveld, J., and
 393 Pozzer, A.: Implementation of a comprehensive ice crystal formation parameterization for cirrus and mixed-phase clouds
 394 in the EMAC model (based on MESSy 2.53), *Geoscientific Model Development*, 11, 4021-4041, 10.5194/gmd-11-4021-
 395 2018, 2018.
- 396 Behera, S. N., Betha, R., Liu, P., and Balasubramanian, R.: A study of diurnal variations of $PM_{2.5}$ acidity and related chemical
 397 species using a new thermodynamic equilibrium model, *Science of The Total Environment*, 452-453, 286-295,
 398 <https://doi.org/10.1016/j.scitotenv.2013.02.062>, 2013.
- 399 Bouwman, A. F., Lee, D. S., Asman, W. A. H., Dentener, F. J., VanderHoek, K. W., and Olivier, J. G. J.: A global high-
 400 resolution emission inventory for ammonia, *Global Biogeochemical Cycles*, 11, 561-587, 10.1029/97gb02266, 1997.
- 401 Cheng, Y. F., Zheng, G. J., Wei, C., Mu, Q., Zheng, B., Wang, Z. B., Gao, M., Zhang, Q., He, K. B., Carmichael, G., Poschl,
 402 U., and Su, H.: Reactive nitrogen chemistry in aerosol water as a source of sulfate during haze events in China, *Science*
 403 *Advances*, 2, 10.1126/sciadv.1601530, 2016.
- 404 Clegg, S. L., Brimblecombe, P., and Wexler, A. S.: Thermodynamic model of the system $H^+-NH_4^+-Na^+-SO_4^{2-}-NB_3^- -Cl^-$ -
 405 H_2O at 298.15 K, *J. Phys. Chem. A*, 102, 2155-2171, 10.1021/jp973043j, 1998.
- 406 Craig, R. L., Peterson, P. K., Nandy, L., Lei, Z., Hossain, M. A., Camarena, S., Dodson, R. A., Cook, R. D., Dutcher, C. S., and Ault, A. P.:
 407 Direct Determination of Aerosol pH: Size-Resolved Measurements of Submicrometer and Supermicrometer Aqueous Particles,
 408 *Analytical Chemistry*, 90, 11232-11239, 10.1021/acs.analchem.8b00586, 2018.
- 409 Dall'Osto, M., Airs, R. L., Beale, R., Cree, C., Fitzsimons, M. F., Beddows, D., Harrison, R. M., Ceburnis, D., O'Dowd, C.,
 410 Rinaldi, M., Paglione, M., Nenes, A., Decesari, S., and Simó, R.: Simultaneous Detection of Alkylamines in the Surface

411 Ocean and Atmosphere of the Antarctic Sympagic Environment, ACS Earth and Space Chemistry, 3, 854-862,
412 10.1021/acsearthspacechem.9b00028, 2019.

413 Dentener, F., Kinne, S., Bond, T., Boucher, O., Cofala, J., Generoso, S., Ginoux, P., Gong, S., Hoelzemann, J. J., Ito, A.,
414 Marelli, L., Penner, J. E., Putaud, J. P., Textor, C., Schulz, M., van der Werf, G. R., and Wilson, J.: Emissions of primary
415 aerosol and precursor gases in the years 2000 and 1750 prescribed data-sets for AeroCom, Atmos. Chem. Phys., 6, 4321-
416 4344, 2006.

417 Ding, J., Zhao, P., Su, J., Dong, Q., Du, X., and Zhang, Y.: Aerosol pH and its driving factors in Beijing, Atmos. Chem. Phys., 19, 7939-
418 7954, 10.5194/acp-19-7939-2019, 2019.

419 Falkovich, A. H., Graber, E. R., Schkolnik, G., Rudich, Y., Maenhaut, W., and Artaxo, P.: Low molecular weight organic
420 acids in aerosol particles from Rondonia, Brazil, during the biomass-burning, transition and wet periods, Atmospheric
421 Chemistry and Physics, 5, 781-797, 10.5194/acp-5-781-2005, 2005.

422 Fang, T., Guo, H. Y., Zeng, L. H., Verma, V., Nenes, A., and Weber, R. J.: Highly Acidic Ambient Particles, Soluble Metals,
423 and Oxidative Potential: A Link between Sulfate and Aerosol Toxicity, Environmental Science & Technology, 51, 2611-
424 2620, 10.1021/acs.est.6b06151, 2017.

425 Fountoukis, C., and Nenes, A.: ISORROPIA II: a computationally efficient thermodynamic equilibrium model for K^+ - Ca^{2+} -
426 Mg^{2+} - NH_4^+ - Na^+ - SO_4^{2-} - NO_3^- - Cl^- - H_2O aerosols, Atmospheric Chemistry and Physics, 7, 4639-4659, 2007.

427 Fridlind, A. M., and Jacobson, M. Z.: A study of gas-aerosol equilibrium and aerosol pH in the remote marine boundary layer during the
428 First Aerosol Characterization Experiment (ACE 1), Journal of Geophysical Research: Atmospheres, 105, 17325-17340,
429 <https://doi.org/10.1029/2000JD900209>, 2000.

430 Friese, E., and Ebel, A.: Temperature Dependent Thermodynamic Model of the System
431 $H-NH_4^+-Na^+-SO_4^{2-}-NO_3^- -Cl^- -H_2O$, The Journal of Physical Chemistry A, 114, 11595-11631, 10.1021/jp101041j,
432 2010.

433 Grewe, V., Brunner, D., Dameris, M., Grenfell, J. L., Hein, R., Shindell, D., and Staehelin, J.: Origin and variability of upper
434 tropospheric nitrogen oxides and ozone at northern mid-latitudes, Atmospheric Environment, 35, 3421-3433,
435 10.1016/s1352-2310(01)00134-0, 2001.

436 Guo, H., Xu, L., Bougiatioti, A., Cerully, K. M., Capps, S. L., Hite, J. R., Carlton, A. G., Lee, S. H., Bergin, M. H., Ng, N. L.,
437 Nenes, A., and Weber, R. J.: Fine-particle water and pH in the southeastern United States, Atmospheric Chemistry and
438 Physics, 15, 5211-5228, 10.5194/acp-15-5211-2015, 2015.

439 Guo, H., Sullivan, A. P., Campuzano-Jost, P., Schroder, J. C., Lopez-Hilfiker, F. D., Dibb, J. E., Jimenez, J. L., Thornton, J.
440 A., Brown, S. S., Nenes, A., and Weber, R. J.: Fine particle pH and the partitioning of nitric acid during winter in the
441 northeastern United States, Journal of Geophysical Research-Atmospheres, 121, 10355-10376, 10.1002/2016jd025311,
442 2016.

443 Guo, H., Otjes, R., Schlag, P., Kiendler-Scharr, A., Nenes, A., and Weber, R. J.: Effectiveness of ammonia reduction on control
444 of fine particle nitrate, Atmospheric Chemistry and Physics, 18, 12241-12256, 10.5194/acp-18-12241-2018, 2018.

445 Guo, H. Y., Liu, J. M., Froyd, K. D., Roberts, J. M., Veres, P. R., Hayes, P. L., Jimenez, J. L., Nenes, A., and Weber, R. J.:
446 Fine particle pH and gas-particle phase partitioning of inorganic species in Pasadena, California, during the 2010 CalNex
447 campaign, Atmospheric Chemistry and Physics, 17, 5703-5719, 10.5194/acp-17-5703-2017, 2017.

448 He, K., Zhao, Q., Ma, Y., Duan, F., Yang, F., Shi, Z., and Chen, G.: Spatial and seasonal variability of $PM_{2.5}$ acidity at two
449 Chinese megacities: insights into the formation of secondary inorganic aerosols, Atmos. Chem. Phys., 12, 1377-1395, 10.5194/acp-12-
450 1377-2012, 2012.

451 He, P., Alexander, B., Geng, L., Chi, X., Fan, S., Zhan, H., Kang, H., Zheng, G., Cheng, Y., Su, H., Liu, C., and Xie, Z.: Isotopic constraints
452 on heterogeneous sulfate production in Beijing haze, Atmos. Chem. Phys., 18, 5515-5528, 10.5194/acp-18-5515-2018, 2018.

453 Hennigan, C. J., Izumi, J., Sullivan, A. P., Weber, R. J., and Nenes, A.: A critical evaluation of proxy methods used to estimate
454 the acidity of atmospheric particles, Atmospheric Chemistry and Physics, 15, 2775-2790, 10.5194/acp-15-2775-2015,
455 2015.

456 Jacob, D. J.: Heterogeneous chemistry and tropospheric ozone, Atmospheric Environment, 34, 2131-2159, 10.1016/s1352-
457 2310(99)00462-8, 2000.

458 Jensen, J.: On the convex functions and inequalities between mean values, Acta Mathematica, 30, 175-193,
459 10.1007/bf02418571, 1906.

460 Jia, S., Wang, X., Zhang, Q., Sarkar, S., Wu, L., Huang, M., Zhang, J., and Yang, L.: Technical note: Comparison and
461 interconversion of pH based on different standard states for aerosol acidity characterization, *Atmos. Chem. Phys.*, 18,
462 11125-11133, 10.5194/acp-18-11125-2018, 2018.

463 Jickells, T. D., An, Z. S., Andersen, K. K., Baker, A. R., Bergametti, G., Brooks, N., Cao, J. J., Boyd, P. W., Duce, R. A.,
464 Hunter, K. A., Kawahata, H., Kubilay, N., laRoche, J., Liss, P. S., Mahowald, N., Prospero, J. M., Ridgwell, A. J., Tegen,
465 I., and Torres, R.: Global iron connections between desert dust, ocean biogeochemistry, and climate, *Science*, 308, 67-71,
466 10.1126/science.1105959, 2005.

467 Jöckel, P., Tost, H., Pozzer, A., Bruehl, C., Buchholz, J., Ganzeveld, L., Hoor, P., Kerkweg, A., Lawrence, M. G., Sander, R.,
468 Steil, B., Stiller, G., Tanarhte, M., Taraborrelli, D., Van Aardenne, J., and Lelieveld, J.: The atmospheric chemistry general
469 circulation model ECHAM5/MESSy1: consistent simulation of ozone from the surface to the mesosphere, *Atmos. Chem.*
470 *Phys.*, 6, 5067-5104, 2006.

471 Jöckel, P., Kerkweg, A., Pozzer, A., Sander, R., Tost, H., Riede, H., Baumgaertner, A., Gromov, S., and Kern, B.: Development
472 cycle 2 of the Modular Earth Submodel System (MESSy2), *Geoscientific Model Development*, 3, 717-752, 2010.

473 Karydis, V. A., Tsimpidi, A. P., Pozzer, A., Astitha, M., and Lelieveld, J.: Effects of mineral dust on global atmospheric nitrate
474 concentrations, *Atmos. Chem. Phys.*, 16, 1491-1509, 10.5194/acp-16-1491-2016, 2016.

475 Karydis, V. A., Tsimpidi, A. P., Bacer, S., Pozzer, A., Nenes, A., and Lelieveld, J.: Global impact of mineral dust on cloud
476 droplet number concentration, *Atmospheric Chemistry and Physics*, 17, 5601-5621, 10.5194/acp-17-5601-2017, 2017.

477 Kerkweg, A., Buchholz, J., Ganzeveld, L., Pozzer, A., Tost, H., and Jöckel, P.: Technical Note: An implementation of the dry
478 removal processes DRY DEPosition and SEDimentation in the Modular Earth Submodel System (MESSy), *Atmos. Chem.*
479 *Phys.*, 6, 4617-4632, 2006.

480 Klingmüller, K., Metzger, S., Abdelkader, M., Karydis, V. A., Stenchikov, G. L., Pozzer, A., and Lelieveld, J.: Revised mineral
481 dust emissions in the atmospheric chemistry-climate model EMAC (MESSy 2.52 DU_Astitha1 KKDU2017 patch),
482 *Geoscientific Model Development*, 11, 989-1008, 10.5194/gmd-11-989-2018, 2018.

483 Klingmüller, K., Lelieveld, J., Karydis, V. A., and Stenchikov, G. L.: Direct radiative effect of dust-pollution interactions,
484 *Atmospheric Chemistry and Physics*, 19, 7397-7408, 10.5194/acp-19-7397-2019, 2019.

485 Klingmüller, K., Karydis, V. A., Bacer, S., Stenchikov, G. L., and Lelieveld, J.: Weaker cooling by aerosols due to dust-
486 pollution interactions, *Atmos. Chem. Phys. Discuss.*, 2020, 1-19, 10.5194/acp-2020-531, 2020.

487 Lawal, A. S., Guan, X. B., Liu, C., Henneman, L. R. F., Vasilakos, P., Bhogineni, V., Weber, R. J., Nenes, A., and Russell, A.
488 G.: Linked Response of Aerosol Acidity and Ammonia to SO₂ and NO_x Emissions Reductions in the United States,
489 *Environmental Science & Technology*, 52, 9861-9873, 10.1021/acs.est.8b00711, 2018.

490 Lelieveld, J., Evans, J. S., Fnais, M., Giannadaki, D., and Pozzer, A.: The contribution of outdoor air pollution sources to
491 premature mortality on a global scale, *Nature*, 525, 367-371, 10.1038/nature15371, 2015.

492 Leygraf, C., Wallinder, I. O., Tidblad, J., and Graedel, T.: *Atmospheric Corrosion*, John Wiley & Sons, 2016.

493 Li, C., McLinden, C., Fioletov, V., Krotkov, N., Carn, S., Joiner, J., Streets, D., He, H., Ren, X., Li, Z., and Dickerson, R. R.:
494 India Is Overtaking China as the World's Largest Emitter of Anthropogenic Sulfur Dioxide, *Scientific Reports*, 7, 14304,
495 10.1038/s41598-017-14639-8, 2017.

496 Liu, M., Song, Y., Zhou, T., Xu, Z., Yan, C., Zheng, M., Wu, Z., Hu, M., Wu, Y., and Zhu, T.: Fine particle pH during severe haze episodes
497 in northern China, *Geophysical Research Letters*, 44, 5213-5221, <https://doi.org/10.1002/2017GL073210>, 2017.

498 Lohmann, U., and Ferrachat, S.: Impact of parametric uncertainties on the present-day climate and on the anthropogenic aerosol
499 effect, *Atmos. Chem. Phys.*, 10, 11373-11383, 10.5194/acp-10-11373-2010, 2010.

500 Marais, E. A., Jacob, D. J., Jimenez, J. L., Campuzano-Jost, P., Day, D. A., Hu, W., Krechmer, J., Zhu, L., Kim, P. S., Miller,
501 C. C., Fisher, J. A., Travis, K., Yu, K., Hanisco, T. F., Wolfe, G. M., Arkinson, H. L., Pye, H. O. T., Froyd, K. D., Liao, J.,
502 and McNeill, V. F.: Aqueous-phase mechanism for secondary organic aerosol formation from isoprene: application to the
503 southeast United States and co-benefit of SO₂ emission controls, *Atmospheric Chemistry and Physics*, 16, 1603-1618,
504 10.5194/acp-16-1603-2016, 2016.

505 Masiol, M., Squizzato, S., Formenton, G., Khan, M. B., Hopke, P. K., Nenes, A., Pandis, S. N., Tositti, L., Benetello, F., Visin,
506 F., and Pavoni, B.: Hybrid multiple-site mass closure and source apportionment of PM_{2.5} and aerosol acidity at major
507 cities in the Po Valley, *Science of The Total Environment*, 704, 135287, <https://doi.org/10.1016/j.scitotenv.2019.135287>,
508 2020.

509 McCormick, M. P., Thomason, L. W., and Trepte, C. R.: ATMOSPHERIC EFFECTS OF THE MT-PINATUBO ERUPTION,
510 *Nature*, 373, 399-404, 10.1038/373399a0, 1995.

511 Meng, Z. Y., Seinfeld, J. H., Saxena, P., and Kim, Y. P.: Atmospheric gas-aerosol equilibrium .4. Thermodynamics of
512 carbonates, *Aerosol Science and Technology*, 23, 131-154, 1995.

513 Meng, Z. Y., and Seinfeld, J. H.: Time scales to achieve atmospheric gas-aerosol equilibrium for volatile species, *Atmospheric*
514 *Environment*, 30, 2889-2900, 10.1016/1352-2310(95)00493-9, 1996.

515 Metzger, S., Mihalopoulos, N., and Lelieveld, J.: Importance of mineral cations and organics in gas-aerosol partitioning of
516 reactive nitrogen compounds: case study based on MINOS results, *Atmospheric Chemistry and Physics*, 6, 2549-2567,
517 10.5194/acp-6-2549-2006, 2006.

518 Murphy, J. G., Gregoire, P. K., Tevlin, A. G., Wentworth, G. R., Ellis, R. A., Markovic, M. Z., and VandenBoer, T. C.: Observational
519 constraints on particle acidity using measurements and modelling of particles and gases, *Faraday Discussions*, 200, 379-395,
520 10.1039/C7FD00086C, 2017.

521 Nah, T., Guo, H., Sullivan, A. P., Chen, Y., Tanner, D. J., Nenes, A., Russell, A., Ng, N. L., Huey, L. G., and Weber, R. J.:
522 Characterization of aerosol composition, aerosol acidity, and organic acid partitioning at an agriculturally intensive rural
523 southeastern US site, *Atmos. Chem. Phys.*, 18, 11471-11491, 10.5194/acp-18-11471-2018, 2018.

524 Nenes, A., Pandis, S. N., Weber, R. J., and Russell, A.: Aerosol pH and liquid water content determine when particulate matter
525 is sensitive to ammonia and nitrate availability, *Atmospheric Chemistry and Physics*, 20, 3249-3258, 10.5194/acp-20-3249-
526 2020, 2020.

527 Oakes, M., Ingall, E. D., Lai, B., Shafer, M. M., Hays, M. D., Liu, Z. G., Russell, A. G., and Weber, R. J.: Iron Solubility
528 Related to Particle Sulfur Content in Source Emission and Ambient Fine Particles, *Environmental Science & Technology*,
529 46, 6637-6644, 10.1021/es300701c, 2012.

530 Park, M., Joo, H. S., Lee, K., Jang, M., Kim, S. D., Kim, I., Borlaza, L. J. S., Lim, H., Shin, H., Chung, K. H., Choi, Y.-H.,
531 Park, S. G., Bae, M.-S., Lee, J., Song, H., and Park, K.: Differential toxicities of fine particulate matters from various
532 sources, *Scientific Reports*, 8, 17007, 10.1038/s41598-018-35398-0, 2018.

533 Pathak, R. K., Yao, X. H., and Chan, C. K.: Sampling artifacts of acidity and ionic species in PM_{2.5}, *Environmental Science*
534 *& Technology*, 38, 254-259, 10.1021/es0342244, 2004.

535 Pathak, R. K., Wu, W. S., and Wang, T.: Summertime PM_{2.5} ionic species in four major cities of China: nitrate formation in
536 an ammonia-deficient atmosphere, *Atmos. Chem. Phys.*, 9, 1711-1722, 10.5194/acp-9-1711-2009, 2009.

537 Petters, M. D., and Kreidenweis, S. M.: A single parameter representation of hygroscopic growth and cloud condensation
538 nucleus activity, *Atmospheric Chemistry and Physics*, 7, 1961-1971, 2007.

539 Pozzer, A., Joeckel, P. J., Sander, R., Williams, J., Ganzeveld, L., and Lelieveld, J.: Technical note: the MESSy-submodel
540 AIRSEA calculating the air-sea exchange of chemical species, *Atmos. Chem. Phys.*, 6, 5435-5444, 2006.

541 Pozzer, A., Jockel, P., and Van Aardenne, J.: The influence of the vertical distribution of emissions on tropospheric chemistry,
542 *Atmospheric Chemistry and Physics*, 9, 9417-9432, 2009.

543 Pozzer, A., de Meij, A., Pringle, K. J., Tost, H., Doering, U. M., van Aardenne, J., and Lelieveld, J.: Distributions and regional
544 budgets of aerosols and their precursors simulated with the EMAC chemistry-climate model, *Atmos. Chem. Phys.*, 12,
545 961-987, 2012.

546 Pozzer, A., Tsimpidi, A. P., Karydis, V. A., de Meij, A., and Lelieveld, J.: Impact of agricultural emission reductions on fine-
547 particulate matter and public health, *Atmospheric Chemistry and Physics*, 17, 12813-12826, 10.5194/acp-17-12813-2017,
548 2017.

549 Pringle, K. J., Tost, H., Message, S., Steil, B., Giannadaki, D., Nenes, A., Fountoukis, C., Stier, P., Vignati, E., and Lelieveld,
550 J.: Description and evaluation of GMXe: a new aerosol submodel for global simulations (v1), *Geoscientific Model*
551 *Development*, 3, 391-412, 2010.

552 Pye, H. O. T., Zuend, A., Fry, J. L., Isaacman-VanWertz, G., Capps, S. L., Appel, K. W., Foroutan, H., Xu, L., Ng, N. L., and Goldstein, A.
553 H.: Coupling of organic and inorganic aerosol systems and the effect on gas-particle partitioning in the southeastern US, *Atmos. Chem.*
554 *Phys.*, 18, 357-370, 10.5194/acp-18-357-2018, 2018.

555 Pye, H. O. T., Nenes, A., Alexander, B., Ault, A. P., Barth, M. C., Clegg, S. L., Collett, J. L., Fahey, K. M., Hennigan, C. J.,
556 Herrmann, H., Kanakidou, M., Kelly, J. T., Ku, I. T., McNeill, V. F., Riemer, N., Schaefer, T., Shi, G. L., Tilgner, A.,
557 Walker, J. T., Wang, T., Weber, R., Xing, J., Zaveri, R. A., and Zuend, A.: The acidity of atmospheric particles and clouds,
558 *Atmospheric Chemistry and Physics*, 20, 4809-4888, 10.5194/acp-20-4809-2020, 2020.

559 Raizenne, M., Neas, L. M., Damokosh, A. I., Dockery, D. W., Spengler, J. D., Koutrakis, P., Ware, J. H., and Speizer, F. E.:
560 Health effects of acid aerosols on North American children: Pulmonary function, *Environmental Health Perspectives*, 104,
561 506-514, 10.2307/3432991, 1996.

562 Roeckner, E., Brokopf, R., Esch, M., Giorgetta, M., Hagemann, S., Kornbluh, L., Manzini, E., Schlese, U., and Schulzweida,
563 U.: Sensitivity of simulated climate to horizontal and vertical resolution in the ECHAM5 atmosphere model, *Journal of*
564 *Climate*, 19, 3771-3791, 10.1175/jcli3824.1, 2006.

565 Saiz-Lopez, A., and von Glasow, R.: Reactive halogen chemistry in the troposphere, *Chemical Society Reviews*, 41, 6448-
566 6472, 10.1039/c2cs35208g, 2012.

567 Sander, R.: Compilation of Henry's law constants (version 4.0) for water as solvent, *Atmos. Chem. Phys.*, 15, 4399-4981,
568 10.5194/acp-15-4399-2015, 2015.

569 Sander, R., Baumgaertner, A., Cabrera-Perez, D., Frank, F., Gromov, S., Grooss, J. U., Harder, H., Huijnen, V., Jockel, P.,
570 Karydis, V. A., Niemeyer, K. E., Pozzer, A., Hella, R. B., Schultz, M. G., Taraborrelli, D., and Tauer, S.: The community
571 atmospheric chemistry box model CAABA/MECCA-4.0, *Geoscientific Model Development*, 12, 1365-1385,
572 10.5194/gmd-12-1365-2019, 2019.

573 Schaap, M., van Loon, M., ten Brink, H. M., Dentener, F. J., and Buitjes, P. J. H.: Secondary inorganic aerosol simulations
574 for Europe with special attention to nitrate, *Atmos. Chem. Phys.*, 4, 857-874, 10.5194/acp-4-857-2004, 2004.

575 Seinfeld, J. H., and Pandis, S. N.: *Atmospheric Chemistry and Physics: From Air Pollution to Climate Change*, Second ed.,
576 John Wiley & Sons, Inc., Hoboken, New Jersey, 2006.

577 Shao, J., Chen, Q., Wang, Y., Lu, X., He, P., Sun, Y., Shah, V., Martin, R. V., Philip, S., Song, S., Zhao, Y., Xie, Z., Zhang,
578 L., and Alexander, B.: Heterogeneous sulfate aerosol formation mechanisms during wintertime Chinese haze events: air
579 quality model assessment using observations of sulfate oxygen isotopes in Beijing, *Atmos. Chem. Phys.*, 19, 6107-6123,
580 10.5194/acp-19-6107-2019, 2019.

581 Shi, G., Xu, J., Peng, X., Xiao, Z., Chen, K., Tian, Y., Guan, X., Feng, Y., Yu, H., Nenes, A., and Russell, A. G.: pH of
582 Aerosols in a Polluted Atmosphere: Source Contributions to Highly Acidic Aerosol, *Environmental Science & Technology*,
583 51, 4289-4296, 10.1021/acs.est.6b05736, 2017.

584 Song, S., Gao, M., Xu, W., Shao, J., Shi, G., Wang, S., Wang, Y., Sun, Y., and McElroy, M. B.: Fine-particle pH for Beijing
585 winter haze as inferred from different thermodynamic equilibrium models, *Atmos. Chem. Phys.*, 18, 7423-7438,
586 10.5194/acp-18-7423-2018, 2018.

587 Squizzato, S., Masiol, M., Brunelli, A., Pistollato, S., Tarabotti, E., Rampazzo, G., and Pavoni, B.: Factors determining the
588 formation of secondary inorganic aerosol: a case study in the Po Valley (Italy), *Atmos. Chem. Phys.*, 13, 1927-1939,
589 10.5194/acp-13-1927-2013, 2013.

590 Sullivan, R. C., Moore, M. J. K., Petters, M. D., Kreidenweis, S. M., Roberts, G. C., and Prather, K. A.: Effect of chemical
591 mixing state on the hygroscopicity and cloud nucleation properties of calcium mineral dust particles, *Atmospheric*
592 *Chemistry and Physics*, 9, 3303-3316, 2009.

593 Surratt, J. D., Chan, A. W. H., Eddingsaas, N. C., Chan, M. N., Loza, C. L., Kwan, A. J., Hersey, S. P., Flagan, R. C., Wennberg,
594 P. O., and Seinfeld, J. H.: Reactive intermediates revealed in secondary organic aerosol formation from isoprene,
595 *Proceedings of the National Academy of Sciences of the United States of America*, 107, 6640-6645,
596 10.1073/pnas.0911114107, 2010.

597 Tan, T., Hu, M., Li, M., Guo, Q., Wu, Y., Fang, X., Gu, F., Wang, Y., and Wu, Z.: New insight into PM2.5 pollution patterns
598 in Beijing based on one-year measurement of chemical compositions, *Science of The Total Environment*, 621, 734-743,
599 <https://doi.org/10.1016/j.scitotenv.2017.11.208>, 2018.

600 Tao, Y., and Murphy, J. G.: The sensitivity of PM2.5 acidity to meteorological parameters and chemical composition changes: 10-year
601 records from six Canadian monitoring sites, *Atmos. Chem. Phys.*, 19, 9309-9320, 10.5194/acp-19-9309-2019, 2019.

602 Tost, H., Jockel, P. J., Kerkweg, A., Sander, R., and Lelieveld, J.: Technical note: A new comprehensive SCAVenging
603 submodel for global atmospheric chemistry modelling, *Atmos. Chem. Phys.*, 6, 565-574, 2006.

604 Tsimpidi, A. P., Karydis, V. A., Pozzer, A., Pandis, S. N., and Lelieveld, J.: ORACLE (v1.0): module to simulate the organic
605 aerosol composition and evolution in the atmosphere, *Geoscientific Model Development*, 7, 3153-3172, 10.5194/gmd-7-
606 3153-2014, 2014.

607 Tsimpidi, A. P., Karydis, V. A., Pandis, S. N., and Lelieveld, J.: Global combustion sources of organic aerosols: model
608 comparison with 84 AMS factor-analysis data sets, *Atmos. Chem. Phys.*, 16, 8939-8962, 10.5194/acp-16-8939-2016, 2016.

609 Tsimpidi, A. P., Karydis, V. A., Pozzer, A., Pandis, S. N., and Lelieveld, J.: ORACLE 2-D (v2.0): an efficient module to
610 compute the volatility and oxygen content of organic aerosol with a global chemistry-climate model, *Geoscientific Model*
611 *Development*, 11, 3369-3389, 10.5194/gmd-11-3369-2018, 2018.

612 van Vuuren, D. P., Edmonds, J., Kainuma, M., Riahi, K., Thomson, A., Hibbard, K., Hurtt, G. C., Kram, T., Krey, V.,
613 Lamarque, J. F., Masui, T., Meinshausen, M., Nakicenovic, N., Smith, S. J., and Rose, S. K.: The representative
614 concentration pathways: an overview, *Climatic Change*, 109, 5-31, 10.1007/s10584-011-0148-z, 2011.

615 Vieira-Filho, M., Pedrotti, J. J., and Fornaro, A.: Water-soluble ions species of size-resolved aerosols: Implications for the
616 atmospheric acidity in São Paulo megacity, Brazil, *Atmospheric Research*, 181, 281-287,
617 <https://doi.org/10.1016/j.atmosres.2016.07.006>, 2016.

618 Vignati, E., Wilson, J., and Stier, P.: M7: An efficient size-resolved aerosol microphysics module for large-scale aerosol
619 transport models, *J. Geophys. Res.-Atmos.*, 109, doi: 10.1029/2003jd004485, 2004.

620 Wang, H., Ding, J., Xu, J., Wen, J., Han, J., Wang, K., Shi, G., Feng, Y., Ivey, C. E., Wang, Y., Nenes, A., Zhao, Q., and
621 Russell, A. G.: Aerosols in an arid environment: The role of aerosol water content, particulate acidity, precursors, and
622 relative humidity on secondary inorganic aerosols, *Science of The Total Environment*, 646, 564-572,
623 <https://doi.org/10.1016/j.scitotenv.2018.07.321>, 2019a.

624 Wang, G., Zhang, R., Gomez, M. E., Yang, L., Levy Zamora, M., Hu, M., Lin, Y., Peng, J., Guo, S., Meng, J., Li, J., Cheng, C., Hu, T., Ren,
625 Y., Wang, Y., Gao, J., Cao, J., An, Z., Zhou, W., Li, G., Wang, J., Tian, P., Marrero-Ortiz, W., Secretst, J., Du, Z., Zheng, J., Shang, D.,
626 Zeng, L., Shao, M., Wang, W., Huang, Y., Wang, Y., Zhu, Y., Li, Y., Hu, J., Pan, B., Cai, L., Cheng, Y., Ji, Y., Zhang, F., Rosenfeld,
627 D., Liss, P. S., Duce, R. A., Kolb, C. E., and Molina, M. J.: Persistent sulfate formation from London Fog to Chinese haze, *Proc Natl
628 Acad Sci U S A*, 113, 13630-13635, 10.1073/pnas.1616540113, 2016.

629 Wang, Y., Li, W., Gao, W., Liu, Z., Tian, S., Shen, R., Ji, D., Wang, S., Wang, L., Tang, G., Song, T., Cheng, M., Wang, G.,
630 Gong, Z., Hao, J., and Zhang, Y.: Trends in particulate matter and its chemical compositions in China from 2013–2017,
631 *Science China Earth Sciences*, 62, 1857-1871, 10.1007/s11430-018-9373-1, 2019b.

632 Weber, R. J., Guo, H. Y., Russell, A. G., and Nenes, A.: High aerosol acidity despite declining atmospheric sulfate
633 concentrations over the past 15 years, *Nature Geoscience*, 9, 282-285, 10.1038/ngeo2665, 2016.

634 Xu, L., Guo, H. Y., Boyd, C. M., Klein, M., Bougiatioti, A., Cerully, K. M., Hite, J. R., Isaacman-VanWertz, G., Kreisberg,
635 N. M., Knote, C., Olson, K., Koss, A., Goldstein, A. H., Hering, S. V., de Gouw, J., Baumann, K., Lee, S. H., Nenes, A.,
636 Weber, R. J., and Ng, N. L.: Effects of anthropogenic emissions on aerosol formation from isoprene and monoterpenes in
637 the southeastern United States, *Proceedings of the National Academy of Sciences of the United States of America*, 112,
638 37-42, 10.1073/pnas.1417609112, 2015.

639 Xue, J., Lau, A. K. H., and Yu, J. Z.: A study of acidity on PM_{2.5} in Hong Kong using online ionic chemical composition
640 measurements, *Atmospheric Environment*, 45, 7081-7088, <https://doi.org/10.1016/j.atmosenv.2011.09.040>, 2011.

641 Yao, X., Ling, T. Y., Fang, M., and Chan, C. K.: Size dependence of in situ pH in submicron atmospheric particles in Hong
642 Kong, *Atmospheric Environment*, 41, 382-393, <https://doi.org/10.1016/j.atmosenv.2006.07.037>, 2007.

643 Yienger, J. J., and Levy, H.: Empirical-model of global soil-biogenic NO_x emissions, *Journal of Geophysical Research-
644 Atmospheres*, 100, 11447-11464, 10.1029/95jd00370, 1995.

645 Zakoura, M., Kakavas, S., Nenes, A., and Pandis, S. N.: Size-resolved aerosol pH over Europe during summer, *Atmos. Chem.
646 Phys. Discuss.*, 2020, 1-24, 10.5194/acp-2019-1146, 2020.

647 Zheng, G., Su, H., Wang, S., Andreae, M. O., Pöschl, U., and Cheng, Y.: Multiphase buffer theory explains contrasts in
648 atmospheric aerosol acidity, *Science*, 369, 1374-1377, 10.1126/science.aba3719, 2020.

650

651 **Author contributions:** V.A.K. and J.L. planned the research, V.A.K., A.P.T. and A.P. performed the model calculations,
652 V.A.K., A.P., and J.L. analyzed the results, V.A.K. and J.L. wrote the paper. All authors contributed to the manuscript.;

653 **Competing interests:** Authors declare no competing interests. **Code/Data availability:** Data and related material can be
654 obtained from V.A.K. (v.karydis@fz-juelich.de) upon request. **Acknowledgments:** The authors gratefully acknowledge the
655 computing time granted on the supercomputer GAIA at Max Planck Institute for Chemistry, Mainz, and on the supercomputer
656 JURECA through JARA at Forschungszentrum Jülich. The work of V.A.K. is supported by the European Union via its Horizon
657 2020 project FORCeS (GA 821205).

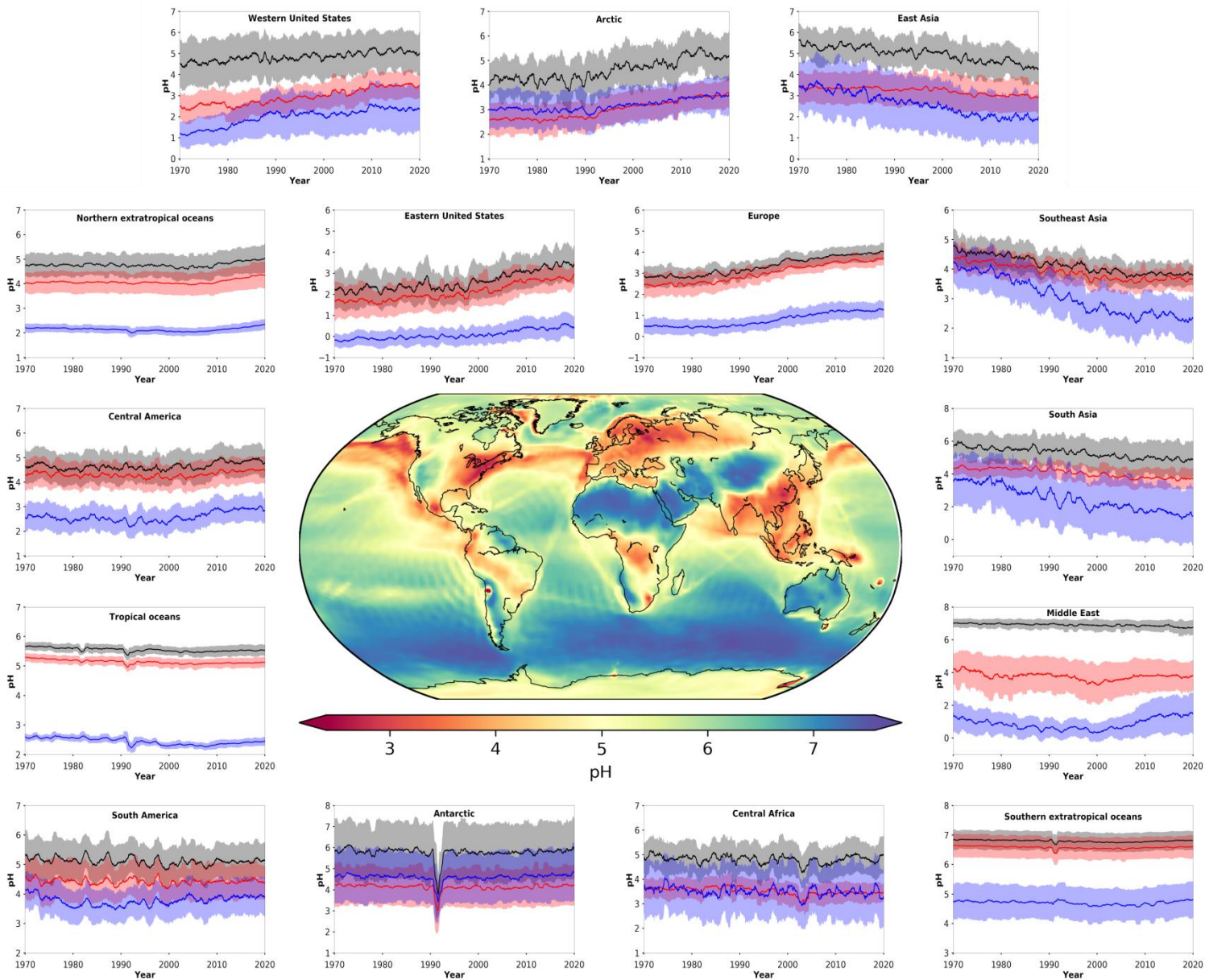
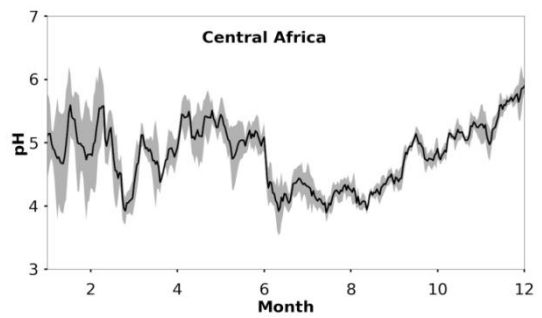
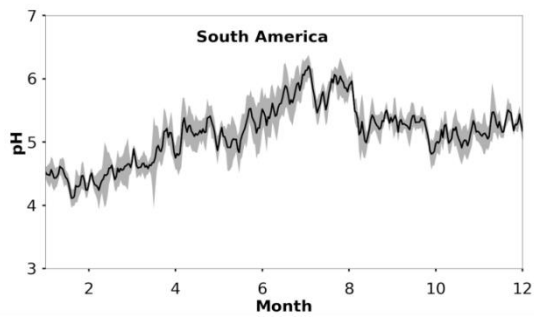
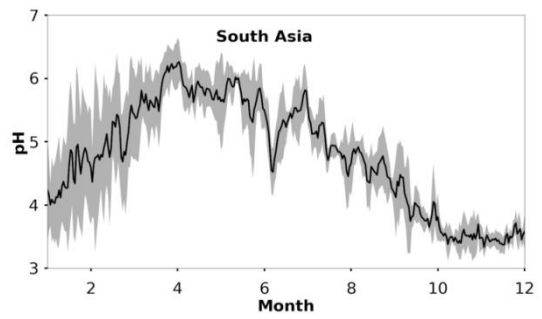
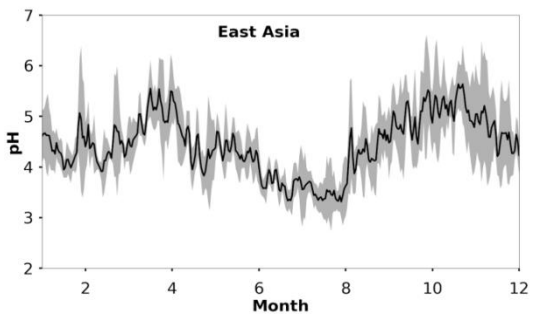
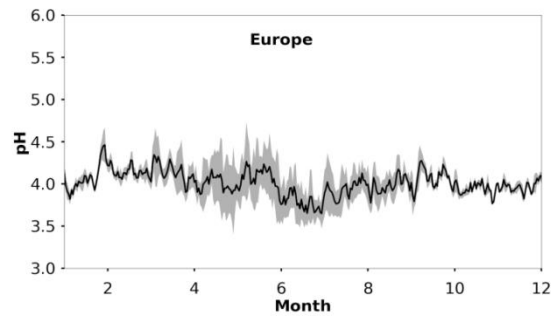
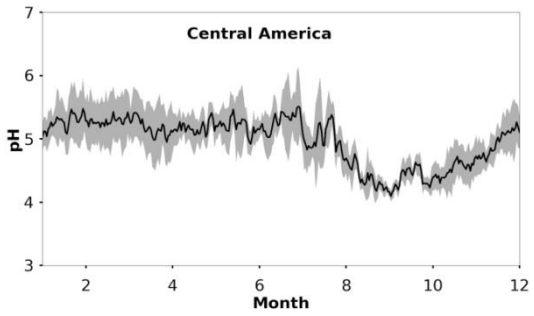
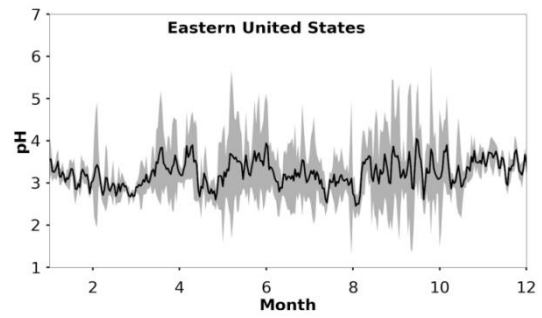
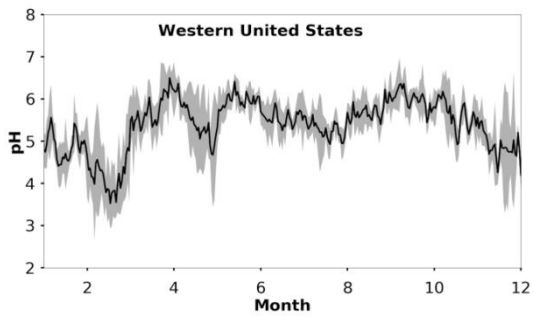


Figure 1: Mean, near-surface fine aerosol particle pH during the period 2010-2015 (central panel). Surrounding panels show the temporal pH evolution during the period 1970-2020 at locations defined in Table 1. Black lines represent the reference simulation. Red and blue lines show the sensitivity simulations in which crustal particle and NH_3 emissions are removed, respectively. Ranges represent the 1σ standard deviation. The anomaly in 1991/2 is related to the Mt Pinatubo eruption.



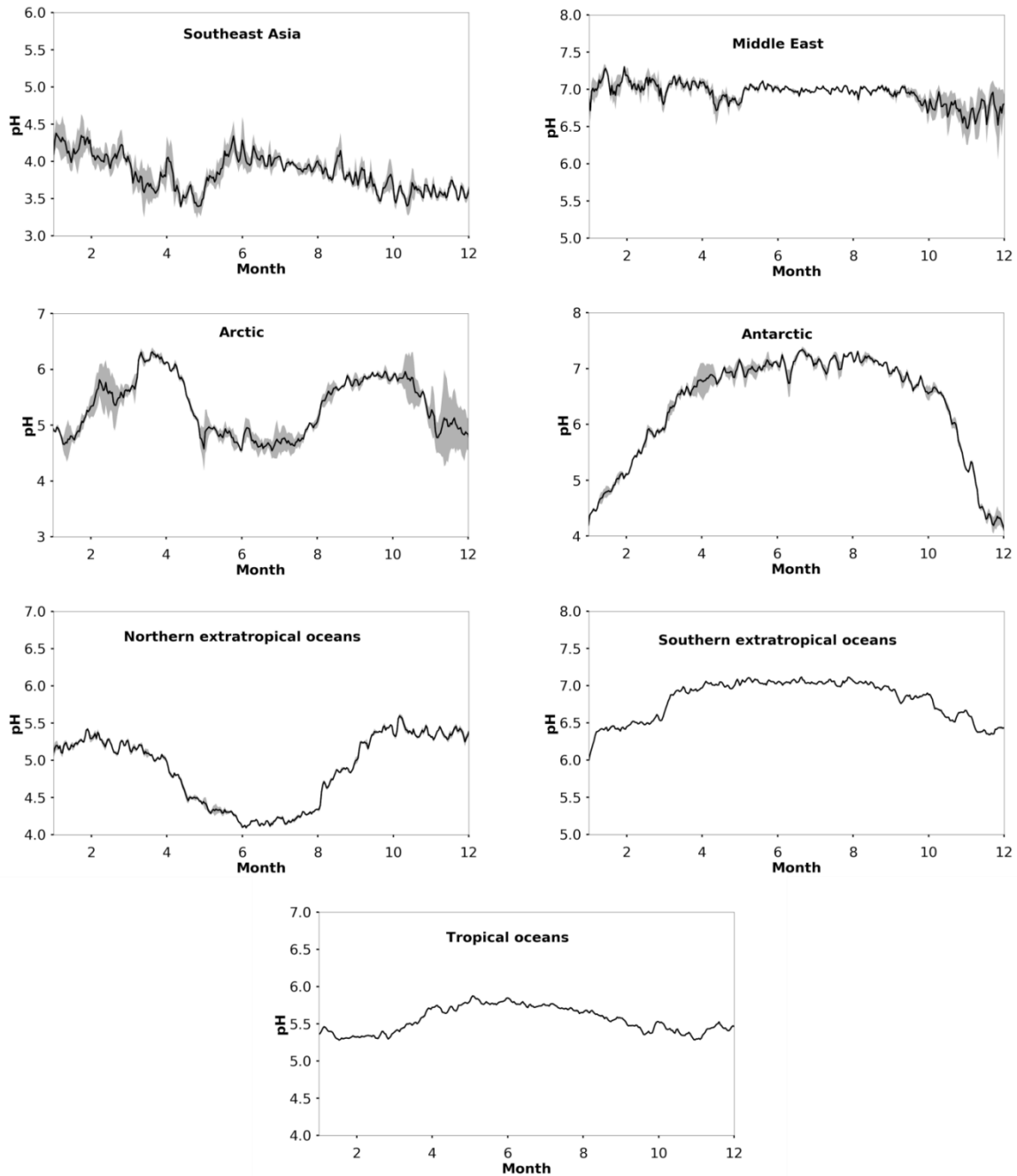


Figure 2: Average seasonal cycle of modelled pH during the period 2010-2015 at locations defined in Table 1. Ranges represent the 1σ standard deviation.

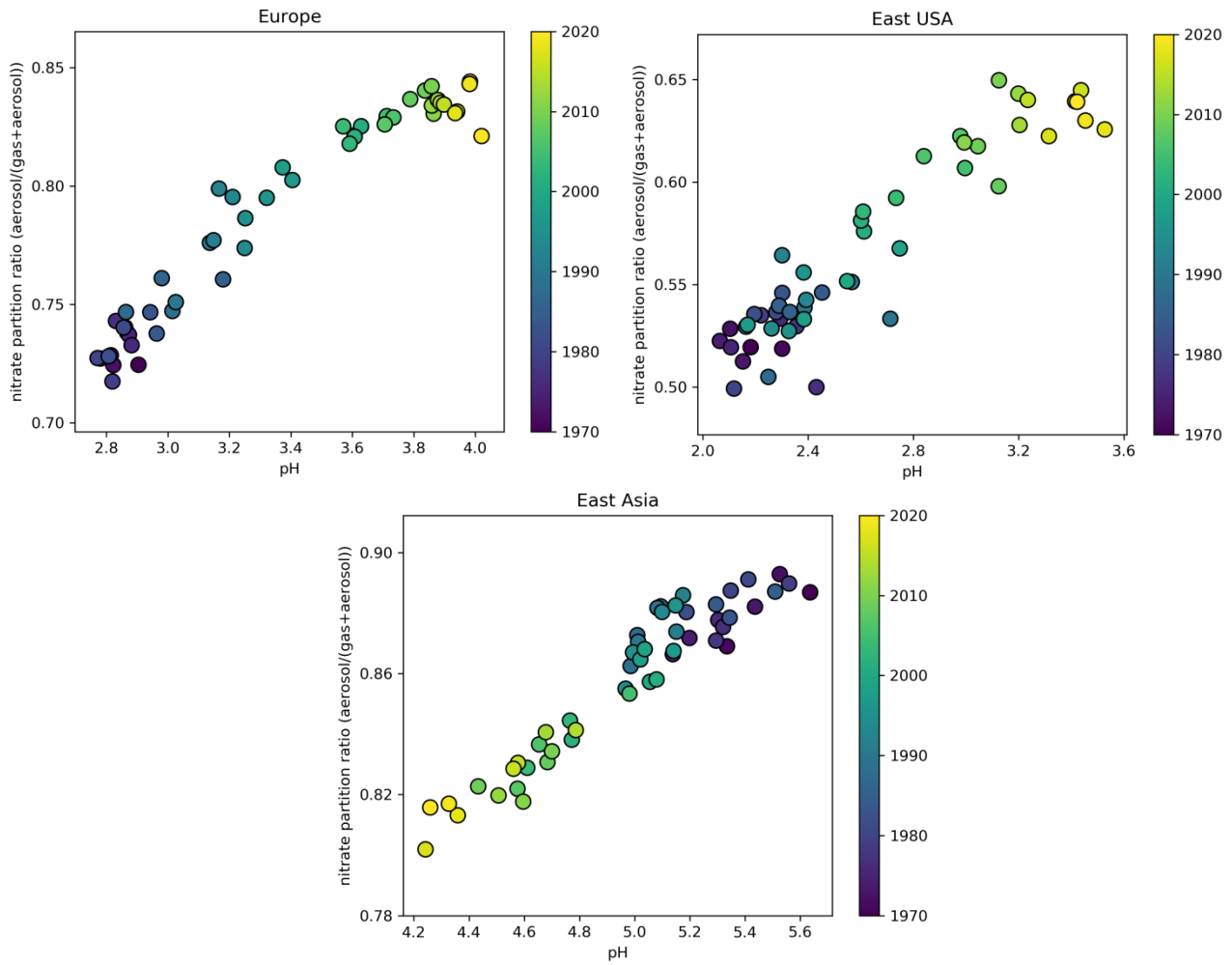


Figure 3: Time evolution of particle phase fraction of total nitrate as a function of pH over Europe (left), the Eastern USA (right) and East Asia (bottom) during the period 1970-2020.

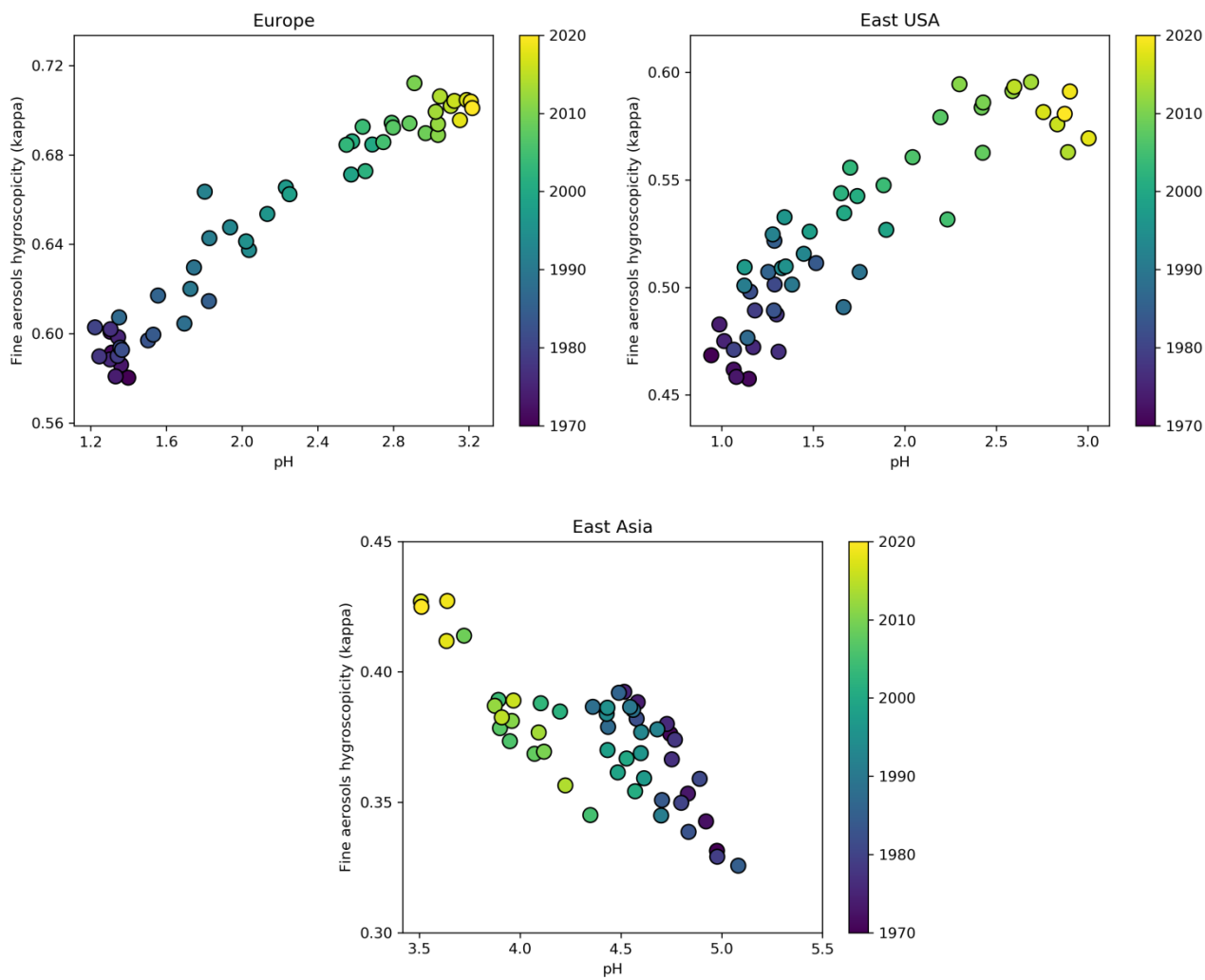


Figure 4: Time evolution of annual average aerosol hygroscopicity (κ) as a function of pH over Europe (left), the Eastern USA (right) and East Asia (bottom) during the period 1970-2020 at the lowest cloud-forming level (940 hPa).

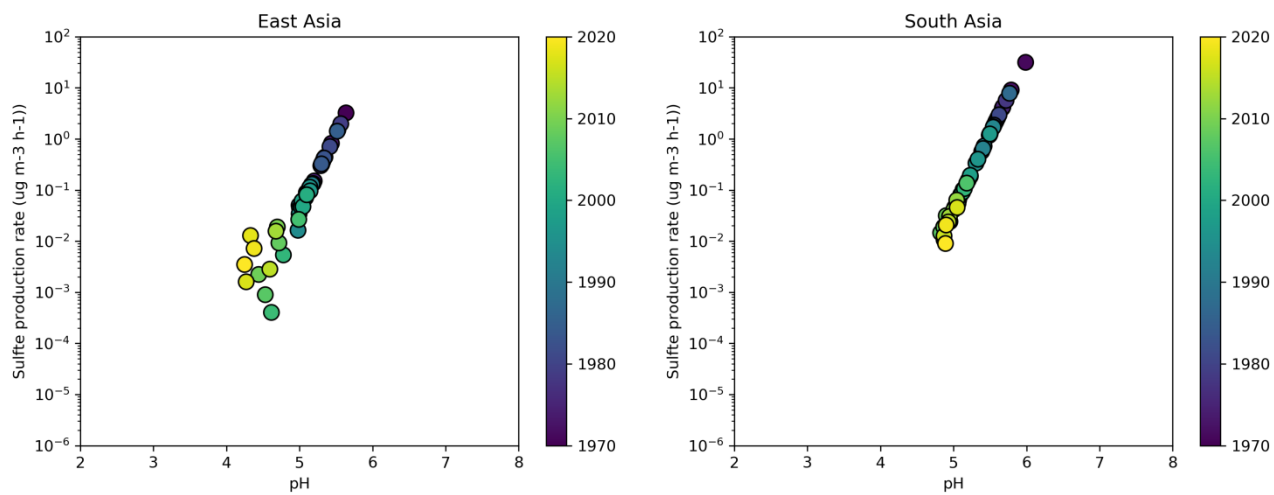


Figure 5: Time evolution of the sulfate production rate on aqueous particles from the $\text{SO}_2 + \text{O}_3$ multiphase chemistry reaction as a function of aerosol particle pH over East Asia (left) and South Asia (right) during the period 1970-2020.

Table 1: Decadal averages of aerosol particle pH.

Region	Longitude	Latitude	1971-1980	1981-1990	1991-2000	2001-2010	2011-2020
Western USA ¹	90°-70°W	30°-46°N	4.6	4.8	4.8	5.0	5.1
Eastern USA ¹	124°-114°W	30°-52°N	2.2	2.4	2.4	2.9	3.3
Central America ¹	106°-52°W	4°-28°N	4.6	4.6	4.6	4.7	4.9
Europe ¹	12°W-36°E	34°-62°N	2.8	3.0	3.3	3.7	3.9
East Asia ¹	100°-114°E	20°-44°N	5.3	5.2	5.1	4.7	4.5
South Asia ¹	68°-94°E	8°-32°N	5.6	5.5	5.3	5.0	4.9
South America ¹	75°-35°W	30°-0°S	5.2	5.1	5.1	5.1	5.1
Central Africa ¹	10°-40°E	10°S-10°N	4.9	4.8	4.8	4.7	4.9
Southeast Asia ¹	94°-130°E	12°S-20°N	4.5	4.3	4.1	3.9	3.8
Middle East ¹	36°-60°E	12°-34°N	7.0	7.0	6.9	6.9	6.8
Arctic	0°-360°	60°-90°N	4.2	4.2	4.6	4.8	5.2
North extratropics ²	0°-360°	20°-60°N	4.8	4.8	4.7	4.7	4.9
Tropical oceans ²	0°-360°	20°S-20°N	5.6	5.6	5.5	5.5	5.5
South extratropics ²	0°-360°	60°-20°S	6.8	6.8	6.8	6.8	6.8
Antarctic	0°-360°	90°-60°S	5.9	5.9	5.6	5.8	5.8

¹Only values over land are considered for the calculation of pH

²Only values over oceans are considered for the calculation of pH

Table A1: Simulated fine aerosol particle pH compared to observationally-constrained estimates of fine particle acidity compiled by Pye et al. (2020).

Location	Latitude	Longitude	Time period	Simulated mean pH (Stable)	Simulated mean pH (Metastable)	Field derived mean pH	Method used	Reference
Pellston, MI, USA	45.55°N	84.78°W	Jul 2016	3.8	3.1	3.5	pH indicator paper/colorimetric image	Craig et al. (2018)
Ann Arbor, MI, USA	42.28°N	83.74°W	Aug 2016	4.3	3.0	3.5	pH indicator paper/colorimetric image	Craig et al. (2018)
Centreville, AL, USA	32.9°N	87.25°W	Jun 1998 – Aug 2013	6.4	5.7	1.2	ISORROPIA (no NH ₃)	Weber et al. (2016)
Centreville, AL, USA	32.9°N	87.25°W	Jun – Jul 2013	7.0	6.5	1.1	ISORROPIA	Pye et al. (2018)
Egbert, ON, Canada	44.23°N	79.78°W	Jul – Sep 2012	3.9	3.5	2.1	E-AIM Model II	Murphy et al. (2017)
Harrow, ON, Canada	42.03°N	82.89°W	Jun – Jul 2007	4.2	3.0	1.6	E-AIM Model II	Murphy et al. (2017)
Pasadena, CA, USA	34.14°N	118.12°W	Jun 2010	5.9	2.7	2.7	ISORROPIA (metastable)	Guo et al. (2017)
Toronto, Canada	43.66°N	79.40°W	2007-2013	4.0	3.6	2.6	E-AIM I (with gas NH ₃ , HNO ₃)	Tao and Murphy (2019)
Toronto, Canada	43.66°N	79.40°W	2014-2016	4.1	3.7	2.7	E-AIM I (with gas NH ₃ , HNO ₃)	Tao and Murphy (2019)
Ottawa, Canada	45.43°N	75.68°W	2007-2016	4.0	3.9	2.5	E-AIM I (with gas NH ₃ , HNO ₃)	Tao and Murphy (2019)
Simcoe, Canada	42.86°N	80.27°W	2007-2016	4.4	3.7	2.41	E-AIM I (with gas NH ₃ , HNO ₃)	Tao and Murphy (2019)
Montreal, Canada	45.65°N	73.57°W	2007-2016	4.0	3.9	2.4	E-AIM I (with gas NH ₃ , HNO ₃)	Tao and Murphy (2019)
Windsor, Canada	42.29°N	83.07°W	2007-2010	4.4	3.6	2.1	E-AIM I (with gas NH ₃ , HNO ₃)	Tao and Murphy (2019)
Windsor, Canada	42.29°N	83.07°W	2012-2016	4.5	3.7	2.4	E-AIM I (with gas NH ₃ , HNO ₃)	Tao and Murphy (2019)
St. Anicet, Canada	45.12°N	74.29°W	2007-2016	4.0	3.9	2.5	E-AIM I (with gas NH ₃ , HNO ₃)	Tao and Murphy (2019)
Sao Paulo, Brazil	23.55°S	46.63°W	Aug – Sep 2012	6.2	6.1	4.8	E-AIM	Vieira-Filho et al. (2016)
Po Valley, Italy	45.40°N	12.20°E	Mar 2009 – Jan 2010	4.5	3.6	3.1	E-AIM Model IV	Squizzato et al. (2013)

Po Valley, Italy	45.40°N	12.20°E	Spring 2009	4.3	3.7	3.6	E-AIM Model IV	Squizzato et al. (2013)
Po Valley, Italy	45.40°N	12.20°E	Summer 2009	4.8	3.0	2.3	E-AIM Model IV	Squizzato et al. (2013)
Po Valley, Italy	45.40°N	12.20°E	Fall 2009	4.5	3.6	3	E-AIM Model IV	Squizzato et al. (2013)
Po Valley, Italy	45.40°N	12.20°E	Winter 2009-2010	4.4	4.0	3.4	E-AIM Model IV	Squizzato et al. (2013)
Po Valley, Italy	45.40°N	12.20°E	Winter 2012-2013	4.2	4.0	3.9	ISORROPIA (metastable, no NH ₃)	Masiol et al. (2020)
Po Valley, Italy	45.40°N	12.20°E	Spring 2012	4.1	3.1	2.3	ISORROPIA (metastable, no NH ₃)	Masiol et al. (2020)
Cabauw, Netherlands	51.97°N	4.93°E	Jul 2012 – Jun 2013	4.0	3.8	3.7	ISORROPIA	Guo et al. (2018)
Cabauw, Netherlands	51.97°N	4.93°E	Jun – Aug 2013	3.6	3.4	3.3	ISORROPIA	Guo et al. (2018)
Cabauw, Netherlands	51.97°N	4.93°E	Dec – Feb 2012	4.1	4.1	3.9	ISORROPIA	Guo et al. (2018)
Beijing, China	39.99°N	116.30°E	Nov 2015 – Dec 2016	4.9	4.2	4.2	ISORROPIA	Liu et al. (2017)
Guangzhou, China	23.13°N	113.26°E	Jul 2013	2.6	1.9	2.5	E-AIM Model IV	Jia et al. (2018)
Beijing, China	39.97°N	116.37°E	Nov 2014 – Dec 2014	4.5	5.3	4.6	ISORROPIA	Song et al. (2018)
Beijing, China	40.41°N	116.68°E	Oct 2014 – Jan 2015	5.6	4.9	4.7	ISORROPIA (metastable)	He et al. (2018)
Beijing, China	39.99°N	116.31°E	Jan – Dec 2014	4.9	4.0	3.0	ISORROPIA (metastable)	Tan et al. (2018)
Beijing, China	39.99°N	116.31°E	Winter 2014	5.5	4.4	4.1	ISORROPIA (metastable)	Tan et al. (2018)
Beijing, China	39.99°N	116.31°E	Fall 2014	6.0	4.6	3.1	ISORROPIA (metastable)	Tan et al. (2018)
Beijing, China	39.99°N	116.31°E	Spring 2014	5.4	4.5	2.1	ISORROPIA (metastable)	Tan et al. (2018)
Beijing, China	39.99°N	116.31°E	Summer 2014	3.1	2.4	1.8	ISORROPIA (metastable)	Tan et al. (2018)
Tianjin, China	39.11°N	117.16°E	Dec 2014 – Jun 2015	4.4	3.7	4.9	ISORROPIA (metastable)	Shi et al. (2017)
Tianjin, China	39.11°N	117.16°E	Aug 2015	1.4	1.2	3.4	ISORROPIA	Shi et al. (2017)

China							(metastable)	
Beijing, China	39.98°N	116.28°E	Feb 2017	4.7	4.8	4.5	ISORROPIA	Ding et al. (2019)
Beijing, China	39.98°N	116.28°E	Apr - May 2016	5.2	4.7	4.4	ISORROPIA	Ding et al. (2019)
Beijing, China	39.98°N	116.28°E	Jul - Aug 2017	2.2	1.9	3.8	ISORROPIA	Ding et al. (2019)
Beijing, China	39.98°N	116.28°E	Sep - Oct 2017	4.5	3.7	4.3	ISORROPIA	Ding et al. (2019)
Guangzhou, China	23.13°N	113.26°E	Jul – Sep 2013	2.7	2.2	2.4	E-AIM Model III	Jia et al. (2018)
Hohhot, China	40.48°N	111.41°E	Summer 2014	5.5	4.0	5	ISORROPIA (metastable, no NH ₃)	Wang et al., 2019
Hohhot, China	40.48°N	111.41°E	Autumn 2014	6.8	5.3	5.3	ISORROPIA (metastable, no NH ₃)	Wang et al. (2019)
Hohhot, China	40.48°N	111.41°E	Winter 2014	5.8	5.0	5.7	ISORROPIA (metastable, no NH ₃)	Wang et al. (2019)
Hohhot, China	40.48°N	111.41°E	Spring 2015	6.1	5.1	6.1	ISORROPIA (metastable, no NH ₃)	Wang et al. (2019)
Hohhot, China	40.48°N	111.41°E	2014 - 2015	6.2	5.0	5.6	ISORROPIA (metastable, no NH ₃)	Wang et al. (2019)
Beijing, China	40.41°N	116.68°E	Oct 2014 – Jan 2015	5.6	4.9	7.6	ISORROPIA (stable state)	He et al. (2018)
Xi'an, China	34.23°N	108.89°E	Nov – Dec 2012	5.7	4.5	6.7	ISORROPIA	Wang et al. (2016)
Beijing, China	39.99°N	116.30°E	Jan – Feb 2015	5.0	3.8	7.6	ISORROPIA	Wang et al. (2016)
Beijing, China	40.35°N	116.30°E	Jun – Aug 2005	4.2	3.3	0.6	E-AIM Model II (only aerosols)	Pathak et al. (2009)
Shanghai, China	31.45°N	121.10°E	May – Jun 2005	3.5	3.1	0.7	E-AIM Model II (only aerosols)	Pathak et al. (2009)
Lanzhou, China	36.13°N	103.68°E	Jun – Jul 2006	6.8	5.1	0.6	E-AIM Model II (only aerosols)	Pathak et al. (2009)
Beijing, China	40.32°N	116.32°E	Jan 2005 – Apr 2006	5.1	4.1	0.7	E-AIM Model II (only aerosols)	He et al. (2012)
Chongqing, China	29.57°N	106.53°E	Jan 2005 – Apr 2006	3.6	2.7	1.5	E-AIM Model II (only aerosols)	He et al. (2012)
Beijing, China	40°N	116.33°E	Jan 2013	4.6	4.5	5.8	ISORROPIA (forward & reverse, estimated)	Wang et al. (2016)

							NH ₃)	
Singapore	1.3°N	103.78°E	Sep – Nov 2011	3.2	3.0	0.6	E-AIM Model IV	Behera et al. (2013)
Hong Kong	22.34°N	114.26°E	Jul 1997 – May 1998	3.3	3.0	0.3	E-AIM Model II (for RH ≥ 70%)	Yao et al. (2007)
Hong Kong	22.34°N	114.26°E	Nov 1996 – Nov 1997	3.4	2.9	-1	E-AIM Model II (for RH < 70%)	Yao et al. (2007)
Hong Kong	22.34°N	114.26°E	Oct 2008	5.0	3.2	0.6	E-AIM Model III (only aerosols)	Xue et al. (2011)
Hong Kong	22.34°N	114.26°E	Nov 2008	3.7	2.7	-0.5	E-AIM Model III (only aerosols)	Xue et al. (2011)
Hong Kong	22.34°N	114.26°E	Jun - Jul 2009	1.6	2.0	-0.1	E-AIM Model III (only aerosols)	Xue et al. (2011)
Pacific Ocean	47.5°S	147.5°E	Nov - Dec 1995	7.0	6.5	1.0	EQUISOLV	Fridlind and Jacobson (2000)
South Ocean	61°S	45°W	Jan 2015	6.9	6.7	1.4	ISORROPIA (no NH ₃)	Dall'Osto et al. (2019)
South Ocean	64°S	65°W	Jan – Feb 2015	6.9	6.8	3.8	ISORROPIA (no NH ₃)	Dall'Osto et al. (2019)
